Title: Dynamic model of basic oxygen steelmaking process based on multi-zone reaction kinetics: Model derivation and validation

Author 1 (corresponding author)

Name: Bapin Kumar Rout

Affiliation: Faculty of Science, Engineering and Technology, Swinburne University of Technology

Mailing Address: Hawthorn, Victoria, 3122, Australia, Email: brout@swin.edu.au

Phone: +61 3 9214 2837

Author 2

Name: Geoff Brooks

Affiliation: Faculty of Science, Engineering and Technology, Swinburne University of Technology

Mailing Address: Hawthorn, Victoria, 3122, Australia.

Phone: +61 3 9214 5672

Author 3

Name: M. Akbar Rhamdhani

Affiliation: Faculty of Science, Engineering and Technology, Swinburne University of Technology

Mailing Address: Hawthorn, Victoria, 3122, Australia.

Phone: +61 3 9214 8528

Author 4

Name: Zushu Li

Affiliation: WMG, University of Warwick

Mailing Address: WMG, University of Warwick, Coventry, CV4 7AL United Kingdom

Author 5

Name: Frank N. H. Schrama

Affiliation: Tata Steel, Netherlands.

Mailing Address: Building 4H16, PO Box 10000, 1970 CA IJmuiden, NL

Author 6

Name: Jianjun Sun

Affiliation: Tata Steel, Netherlands.

Mailing Address: Building 4H16, PO Box 10000, 1970 CA IJmuiden, NL

Abstract

A multi-zone kinetic model coupled with a dynamic slag generation model was developed for the simulation of hot metal and slag composition during the BOF operation. The three reaction zones, (i) jet impact zone (ii) slag-bulk metal zone (iii) slag-metal-gas emulsion zone were considered for the calculation of overall refining kinetics. In the rate equations, the transient rate parameters were mathematically described as a function of process variables. A micro and macroscopic rate calculation methodology (micro-kinetics and macro-kinetics) were developed to estimate the total refining contributed by the recirculating metal droplets through the slag-metal emulsion zone. The micro-kinetics involves developing the rate equation for individual droplets in the emulsion. The mathematical models for the size distribution of initial droplets, kinetics of simultaneous refining of elements, the residence time in the emulsion, dynamic interfacial area change were established in the micro-kinetic model. In the macro-kinetics calculation, a droplet generation model was employed and the total amount of refining by emulsion was calculated by summing the refining from the entire population of returning droplets. A dynamic Fe_tO generation model based on oxygen mass balance was developed and coupled with the multi-zone kinetic model. The effect of post-combustion on the evolution of slag and metal composition was investigated. The model was applied to a 200-ton top blowing converter and the simulated value of metal and slag was found to be in good agreement with the measured data. The post-combustion ratio was found to be an important factor in controlling Fe_tO content in the slag and the kinetics of Mn and P in a BOF process.

Keywords: BOF, dynamic model, multi-zone kinetics, slag generation model, kinetics

Introduction

The basic oxygen furnace (BOF) has been a leading route of steel production for more than six decades and become mature in terms of safety, stable operation and maximization in productivity. However, nowadays it faces different challenges e.g. strict quality control, minimizing energy cost, maximizing yield and reducing environmental pollution. Focusing on improving the process by developing fundamental understanding and enabling dynamic correction is the crucial step to optimize the BOF process. A dynamic model that can explain the changes in the critical process parameters based on the events taking place in the furnace operation is a must-have tool for the operators. It can be a base to develop an automatic control system of the process. Therefore, in the recent years, there has been an increasing amount of literature focusing on developing computer based dynamic models for the BOF process. [1-13]

Kattenbelt *et al.* [9] developed a dynamic model for BOF based on the measured step response of control variables such as oxygen flow rate, lance height and flux addition. Although the authors discussed the mechanism of decarburization reaction based on the work of droplet generation, the size of droplets and residence time in the emulsion, no fundamental relationship to include these parameters was employed in this work. Li *et al.* [12] applied the three-stage decarburization theory and applied three separate equations to simulate the decarburization rate. The rate equations were modified with the bath mixing degree, which was described as a function of dynamic lance height. The rate constants of the equations were derived by fitting the data from 67 heats. Similar to Kattenbelt *et al.* [9], the dynamic model developed by Li *et al.*, cannot provide a physical insight of the BOF process due to the empiricism involved in deriving the rate parameters.

Understanding that the BOF process rarely attains thermodynamic equilibrium [14], the principle of chemical kinetics has appealed to many researchers in quantitative prediction of the refining rates. Several researchers [6, 7, 10] have applied the "coupled reaction mechanism" developed by Robertson *et al.* [15] to simulate the slag-metal reactions. Pahlevani *et al.* [6] employed the coupled reaction mechanism in a single zone kinetic model with the flux dissolution model to simulate the BOF refining reaction. Ogasawara *et al.*[7] constructed a dynamic model for dephosphorization by combining coupled reaction model with a dynamic Fe_tO generation model. An oxygen balance method combined with the off-gas data was used to predict Fe_tO in the slag during the blow. In the model built by Lytvynyuk *et al.* [10] the coupled reaction model was combined with the thermodynamics and kinetics of involved phases (interfacial surface of iron melt and slag) in one reaction zone to simulate the BOF process. Scrap melting model and flux dissolution model were included in the simulation. The simulated behaviour of metal and slag compositions by the model was validated with the industrial converters of different sizes.

While the above dynamic models based on coupled reaction model found some success in simulating the slag-metal reactions, the biggest challenge in this type of approach is to quantify the rate parameters, especially the slag-metal interfacial area that is a strong function of dynamic process conditions. Due to lack of fundamental basis to quantify rate parameters such as interfacial area, the above kinetic models employed fitting parameters in the model which are derived from the plant-specific data. [8, 10,11, 12]

The major reactions of BOF process are schematically presented in **Fig. 1**. Based on the difference of reaction environments and mass transfer conditions, the primary reactions zones are divided as: (i) jet impact area where the direct reaction between oxygen gas and melt takes place in an extremely hot environment (ii) slag-metal emulsion phase, where the

reaction between metal drops and slag takes place (iii) slag-bulk metal zone, where a permanent phase contact between the slag and bulk metal is realized. Kinetic parameters of the reactions in a zone can be described as a function of interfacial area, temperature and physicochemical nature of phase interactions. Brooks *et al.*[16] argued that the use of simple first order rate is not appropriate for modeling the BOF process and a transient kinetics approach is necessary to describe the multi-phase heterogeneous reactions. A recent publication by Hewage *et al.* [17] by analysing the IMPHOS pilot plant data[18] showed that a single zone with the first order rate equation may be applicable for the simple reaction like Si oxidation, but the compositional change of P, Mn and C cannot be explained by a simple first order kinetics with constant rate parameters. Similarly, Rout *et al.*[19] analyzed the rate of dephosphorization for a 200-tonne converter data and found that the kinetics of dephosphorization depends on the rate at which the droplets refined in the emulsion and therefore considering the interfacial area at the bulk metal and the slag, cannot simply explain the dephosphorization behaviour.

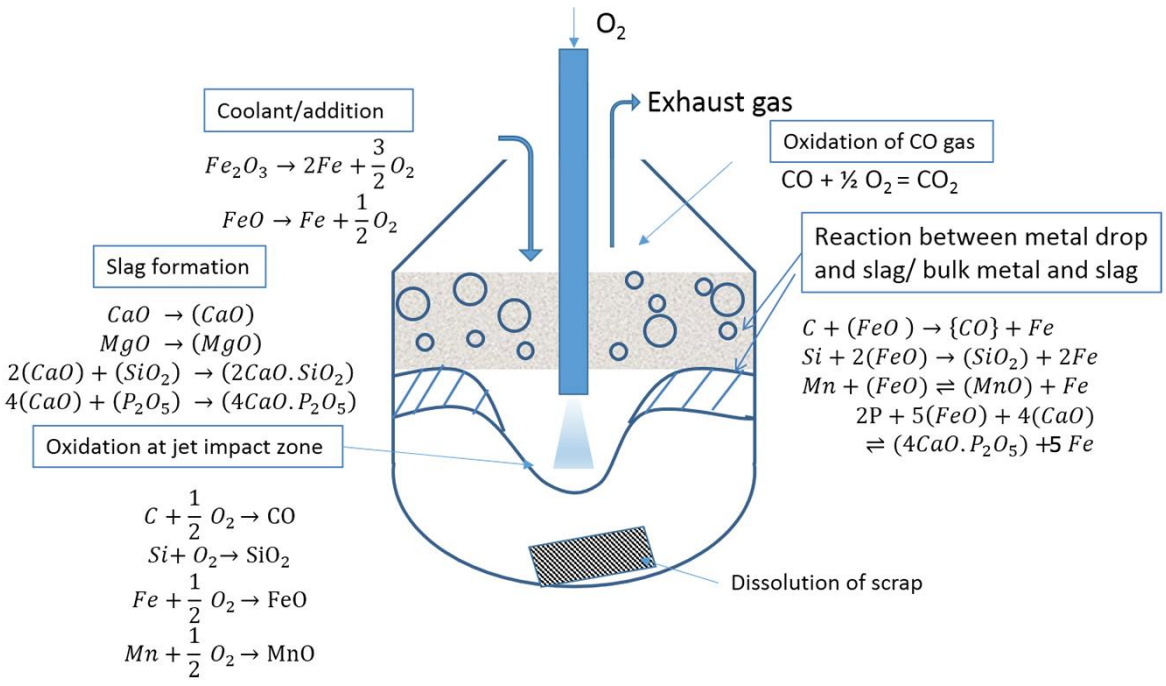

Figure 1: Schematic representation of reactions in BOF converter

Several other researchers developed multi-zone models for BOF process by dividing the converter into several reaction zones. [2, 4, 5] Jalkanen[2] developed a physicochemical model for the BOF process by considering the reaction in three different zones of the converter. In the computational model, the three reaction zones were replaced by a generalized reaction zone and the distribution of oxygen among the various impurities was simulated by their individual reaction affinities expressed by Gibb's reaction energies. The model uses several fixed parameters derived from the plant data and the simulated results are only able to capture the qualitative representation of metal and slag compositions. Dogan *et al.* [6] developed a comprehensive model for decarburization by considering the refining of C in the jet impact and the emulsion zone. The theory of bloated drops in the emulsion and the residence time of the metal drops are successfully incorporated in the model and the model C prediction was found to be consistent with the industrial converter data. However, no FeO prediction model was employed in their study. Sarkar *et al.*'s[8] dynamic model focused on developing a kinetic treatment to the reactions in the emulsion zone. The Gibb's free energy minimization was

applied for simultaneous oxidation kinetics of elements in the metal droplet. In common with Dogan *et al.*, the model was able to incorporate the phenomena of droplet generation, bloating and residence time model in the overall kinetic equation. However, the model prediction of reactions other than C removal was poor, particularly the reversion of Mn and P. A more recent study by Sasaki *et al.*, [13] a three zone kinetic model for industrial BOF operation was employed to predict the metal and slag composition successfully. However, the key model details are not available in the open literature.

The present work has been undertaken to develop a dynamic model for BOF process using the multi-zone kinetic theory. The model attempts to capture most of the physiochemical phenomena of the process by considering three primary refining zones commonly observed in a top blowing process. The ejection of droplets, phenomena of droplet "bloating" due to nucleation of CO gas, and detailed reaction kinetics of droplets for a multicomponent system in the emulsion phase were successfully taken into account in the dynamic model. The overall model was validated with the measured data of a 200-ton industrial converter. The details of the development of the global model and its validation with the industrial data are presented in this paper, while the kinetic models of decarburization and demanganisation are described in separate papers. [20, 21]

1. Model concepts and mathematical formulation

Mathematical treatment to the kinetics of the reactions occurring in each reaction zone has been developed to simulate the overall refining rate of liquid metal. Table 1 shows reaction zones considered for refining of individual impurities in the converter. It is well understood that the removal of phosphorus needs a basic slag due to thermodynamic instability of P_2O_5 at steelmaking temperature. Due to the large impact force exerted by the gas jet on the bath surface, the slag beneath the jet is entirely pushed away from the jet impact zone to the

154 periphery region and the oxygen gas directly reacts with the hot metal.[22] Therefore P
155 removal in the jet impact zone is ignored in this study.

156 The rate equations that describe the refining in the different zones of the converter and the
157 transient kinetic parameters are listed in Table 2.

158 The overall rate of refining can be described by the following equation:

$$\left.\frac{d(W_m C_{jm})}{dt}\right|_{overall}^{t} = \left.\frac{d(W_m C_{jm})}{dt}\right|_{iz}^{t} + \left.\frac{d(W_m C_{jm})}{dt}\right|_{sm}^{t} + \left.\frac{d(W_m C_{jm})}{dt}\right|_{em}^{t} \quad (11)$$

159 **1.1. Jet impact zone**

160 The kinetics of oxidation of Si, Mn in jet impact zone was assumed to be controlled by mass
161 transport in the liquid phase. It is due to rapid dissolution of oxygen in the melt as a result of
162 high temperature prevailing in the hot spot region. The mass transfer coefficient of Si, Mn
163 (k_m^{gm}) in the metal phase has been calculated as a function of stirring energy and geometrical
164 parameters of the furnace (see Appendix A.1).[23] The interfacial concentration C_{im} has been
165 calculated assuming dynamic equilibrium between the reactants and products at the gas/metal
166 interface. The rate parameters for carbon oxidation (k_a and k_g in Eq. 3 and Eq. 4) has been
167 simulated by mixed controlled kinetics, including the gas phase mass transfer and chemical
168 reaction kinetics as rate determining steps.[24] Below a critical level of C the rate of
169 decarburization was assumed to be controlled by carbon diffusion in metal phase. [25,26] It has
170 been reported that the value of critical carbon may lie between 0.3 to 0.8 wt pct depending on
171 the oxygen flow rate. In the present study, a fixed value of critical carbon of 0.3 wt pct was
172 considered. [25,26] The detail mathematical model for C, Si and Mn oxidation kinetics in jet
173 impact zone can be found elsewhere. [20, 21, 27]

The interfacial area was assumed to be the area of the cavity created by the top jet. The surface area of the jet impact was considered to be paraboloid in shape[28] and was calculated as a function of lance height and oxygen flow rate.

$$A_{cav} = \int_0^r 2\pi r_{cav} \left(1+\left(\frac{dh}{dr}\right)^2\right) dr \tag{12}$$

Where A_{cav} is the area of the individual cavity, h is the height and r_{cav} is the radius of the cavity. The analytical solution to Eq. 12 can be expressed as:

$$A_{cav} = \frac{\pi {r_{cav}}^4}{6h^2}\left[\left(1+\frac{4h^2}{{r_{cav}}^2}\right)^{3/2} - 1\right] \tag{13}$$

The height and radius of the cavity were calculated by using the dimensionless correlations suggested by Koria and Lange.[29] The detailed calculation regarding the cavity dimensions is given in Appendix A.2.

It has been observed that the jet cavity formed by each nozzle does not overlap each other when the jet angle exceeds 10 degree. Therefore, in the present work (nozzle angle of 17.5 degree), the total cavity area has been estimated by multiplying individual cavity area by the number of nozzles in the lance tip.

$$A_{iz} = n_n A_{cav} \tag{14}$$

Here n_n is the number of nozzles and A_{iz} is the total surface area of jet impact. The change of cavity shape due to surface oscillation was neglected since it exerts little effect on the final area calculation.[28] The rate equations 1 to 4, described in Table 2, has been employed to determine the weight of refining of C, Si, Mn in the jet impact area.

1.2. Emulsion zone

Many researchers suggested that rapid refining of hot metal in a BOF process proceed via the formation of slag-metal-gas emulsion zone.[18, 30, 31] However, the proportion of refining brought by emulsion zone to the overall bulk metal refining is not clear from the past studies. The mechanism of refining of hot metal by the metal droplet circulation in emulsion zone is schematically illustrated in **Fig. 2**. The droplets ejected from the liquid metal, initially carry the melt concentration and once it remains in contact with the oxidising slag, refining of impurity elements begin to take place. From the laboratory scale study of droplets, it has been observed that the formation of CO either inside or on th surface of the drops as a result of the decarburisation reaction, makes the droplet buoyant and increase the residence time in the emulsion. Fruehan and co-workers[31] were able to capture the phenomena of "bloating" of a metal droplet in a steelmaking type of slag by X-ray fluoroscopy technique. The important aspect of "bloating" is that it increases the residence time of metal droplets in the emulsion, which allows the metal droplets to react with slag for a long period. The continuous creation of large surface area by the formation of small size drops and high reaction time in the emulsion is believed to be a prominent mechanism of BOF refining process. .[18, 30, 31]

The process of refining by emulsion can be visualized in two stages: refining of a single droplet and overall refining by all the droplets. Note that the droplets present in the emulsion at a given blowing time can undergo different physicochemical process depending on their time of the ejection, initial size and residence time. The mathematical treatment to model the refining of bulk metal by the emulsion zone has been divided into two stages:

1. Rate of refining between an individual metal droplet and slag – Microkinetics approach

2. Overall rate of refining by the entire population of the metal droplets – Macrokinetics approach

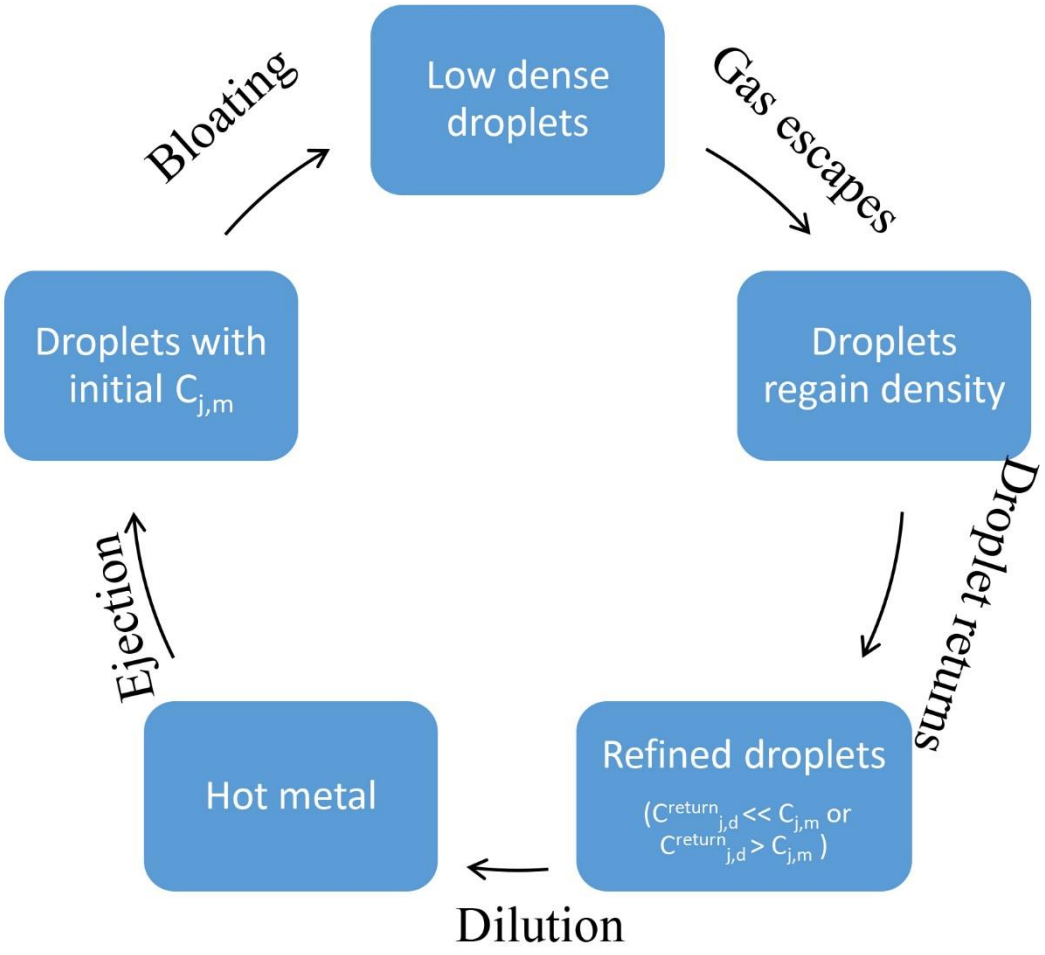

Figure 2: Schematic representation of the refining mechanism in the emulsion zone

1.2.1 Microkinetics of droplet refining in emulsion

The rate equation for refining of elements of a single droplet during the time of residence inside the emulsion can be presented by a first order rate law as presented in Eq. 6 in Table 2. The mathematical treatment to simulate the transient rate parameters such as interfacial area, mass transfer coefficient and interface concentration in the rate equation is presented in the following sections.

1.2.1.1 Simultaneous refining kinetics of impurities

The kinetic model suggested by Brooks *et al*,[32] which uses surface renewal method of carbon diffusion, has been applied to simulate the rate of decarburisation of droplets in the emulsion zone. This approach has been found to be mathermatically reliable in connecting the bloating behaviour of droplets to the overall decarburisation kinetics in the emulsion zone. As suggested by Dogan *et al*.,[6] since there are plenty of oxygen available in the system, the rate of CO formation may be rapid and carbon diffusion can be the rate controlling step for a bloated droplet. While there is no collective agreement regarding the rate determining step of the decarburisation kinetics of droplet, the authors have used the above mentioned approach to connect the bloating phenomena of the droplets to the overall refining of the BOF process. However, further work is necessary to establish an accurate kinetic model for decarburisation.

The fundamental understanding of the simultaneous mass transfer of Si, C, Mn and P across the boundary between the metal droplet and slag interface is limited in the steelmaking literature. There are only a few laboratory scale studies on the kinetics of Fe-C-S[33], Fe-C-P[34, 35], Fe-C-P-S [36]and Fe-C-Si-Mn[37]. The following observations regarding the kinetics of metal droplets in the slag can be made from the past studies:

1. The rate of C removal slows down in the presence of Si and Mn in the droplet.[37]
2. The rate of phosphorus removal is very rapid in the presence of C in the droplet. Phosphorus in the droplet reaches the equilibrium concentration within a few seconds after it enters into the oxidising slag.[34, 35,36]
3. Internal nucleation of CO gas increases the kinetics of P transfer and an increase of S level in the droplet influences the CO formation rate.[38]

Based on these observations, a mechanism of the simultaneous kinetics of C, Si, Mn and P at droplet and slag interface was proposed. According to the proposed reaction mechanism, shown in **Fig. 3**, the oxidation kinetics of Si, P, and Mn proceeds at rapid rate and approaches the equilibrium within a few seconds after the metal drops enters into the emulsion phase. Gaye *et al.* [34]Geiger *et al.*[35] and more recently Gu *et al.*[36] observed that the kinetics of P for Fe-C-P is very rapid and attains the equilibrium value in 10 s. It is further proposed that the quick formation of surface active oxides like SiO_2 and P_2O_5 slow down the kinetics of decarburisation by blocking the reaction sites for C and FeO reaction. The detail calculation of mass transfer coefficient of carbon in the presence of surface active oxides is discussed elsewhere.[20] Carbon refining in a bloated droplet continues until it attains the equilibrium and once the CO gas escapes, the dense and refined drops return to the metal bath.

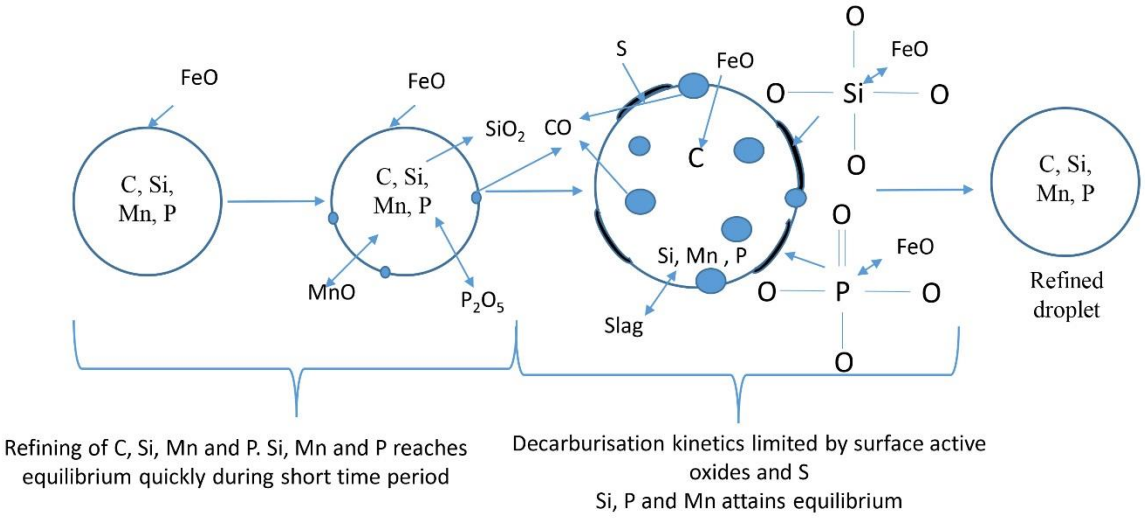

Figure 3: Proposed refining mechanism of metal droplets in the slag-metal emulsion

1.2.1.2 Mass transfer coefficient

Several researchers suggested that Higbie's penetration theory can be used to model the mass transfer coefficient of decarburization rate of a moving metal droplet in the slag-metal emulsion.[32, 39] According to Higbie's theory, it has been assumed that when a metal droplet

moves (ascends, descends or floats) in the slag-metal emulsion domain, the slag packets are brought into contact by turbulent eddy and undergo unsteady state diffusion or penetration by the transferred species during its contact time. For a bubble-agitated stirring system, the calculation of contact time is uncertain, and there is apparently no reliable method available to estimate it. However, for a simple geometry like a spherical droplet which ascends or descends in the slag layer, the contact time can be assumed to be the ratio of diameter to the velocity of the spherical bubble. [39] The mass transfer coefficient in the metal phase can be calculated as:

$$k_{jm}^{d} = 2 \times \sqrt{\frac{D_j}{\pi\, t_c}} = 2 \times \sqrt{\frac{D_j u}{\pi\, d_p}} \qquad (15)$$

Where k_{jm}^{d} is the mass transfer coefficient in metal phase, D_j is the diffusion coefficient of the j^{th} element in metal drop, t_c is the contact time of the slag packet with the metal drop, u is the velocity of the drop and d_p is the average diameter of the drop corresponding to the size class p. The diffusion coefficient of C, Si, Mn and P has been taken from the reported data of solute diffusivity values of elements in the liquid Fe-C alloy at 1873K (see Table 4). Further, the temperature and viscosity effect on mass diffusivity was taken into account by applying the Stokes- Einstein equation.

$$D_T = D_{1873}\left(\frac{T}{1873}\right) \times \left(\frac{\mu_{m,1873}}{\mu_{m,T}}\right) \quad \#(16)$$

Where D_T is the diffusivity at temperature T (m^2/s), D_{1873} is the diffusivity of species at T =1873K (m^2/s), T is the temperature (K), $\mu_{m,1873}$ and $\mu_{m,T}$ are the viscosity of hot metal at 1873K and T respectively. In the present work the effect of temperature on viscosity has been neglected.

On the slag side, it is assumed that the metal droplet is a rigid sphere with the stream of slag surrounding it. Due to high Schmidt number prevailing in steelmaking systems, the boundary layer is considered laminar and the effect of turbulence on mass transfer coefficient can be neglected. According to Oeter[40], the mass transfer coefficient in slag phase (k^d_s) can be determined by the following equation:

$$Sh = 2 + 0.6Re^{1/2}Sc^{1/3} \quad (17)$$

Where Sh is the Sherwood number, Re is the Reynold number and Sc is the Schmidt number. The ion diffusivity in slag, D_{slag} (in Sherwood number calculation) was taken to be 5×10^{-10} m^2/s. [40]

Liquid phase mass transfer control has been assumed for decarburization reaction in the droplets. However, the reactions of Si, Mn and P were assumed to be controlled by both mass transfers in metal and the slag. The overall mass transfer coefficient (k_d^{em}) of the metal droplet in slag, assuming a mixed transport controlled reaction kinetics can be written as: [41]

$$\frac{1}{k_d^{em}} = \frac{1}{k_{jm}^d} + \frac{\rho_m}{k_s^d \rho_s L_j} \quad (18)$$

Here k^d_{jm} and k^d_s are the mass transfer coefficient in metal and slag phase respectively. ρ_m and ρ_s are the densities of metal and slag respectively. L_j is the equilibrium distribution ratio between the slag and metal droplet.

1.2.1.3 Interfacial concentration

The instantaneous equilibrium between the reactants and products has been assumed at the metal drop and slag interface. Slag-bulk metal equilibria were applied to estimate the equilibrium concentration of each component at the metal drop interface. The equilibrium

concentration of carbon was determined by calculating the activity coefficient, concentration and the equilibrium value. It has been observed that both temperature and composition have strong effect on the activity coefficient of C and therefore a polynomial equation of f_c as a function both C and temperature proposed by Chou et al. [25] has been used in this work. The raoulitian activity of iron oxide has been simulated as a function of slag composition and temperature by applying regular solution model.[42] In the case of Si, Mn and P, the equilibrium distribution ratio as a function of the composition and the temperature has been used for the estimation of interfacial concentration

$$[wt\ pct\ C_{ji}] = \frac{(wt\ pct\ C_j)}{L_j} \#(19 \quad)$$

where $[C_{ji}]$ is the concentration (wt pct) at the slag/metal interface, (C_j) is the concentration (wt pct) in the slag and L_j is the equilibrium partition ratio between the metal and slag.

The experimental data reported by Narita *et al.*[43], were used to develop a linear correlation of interfacial Si concentration between the metal and slag as a function of slag FeO (< 40 wt pct). The equilibrium distribution ratio suggested by Suito *et al.*[44], which is valid for CaO-SiO_2-FeO type slag with MnO concentration varying up to 16 wt pct was used to calculate the interfacial manganese concentration. Cicutti *et al.*[45] reported that the equilibrium value of P predicted by the regular solution model agrees well with the oxidation and reversion behaviour of P in an industrial furnace. Thus, in the present work, the P partition ratio was determined by regular solution model. The evaluation of interfacial concentration at the metal drop and slag boundary for various impurities (C, Si, Mn and P) is illustrated in Table 3. The equilibrium distribution ratio models are illustrated in Appendix A.3.

1.2.1.4 Dynamic interfacial area of the droplet

The change in the area and volume of the metal droplet due to bloating phenomena have been estimated by an empirical correlation for density variation as a function of decarburization rate, suggested by Brooks *et al.*[32], based on the experimental measurements by Molloseau and Fruehan[32]:

$$\rho_d = \begin{cases} \rho_{d_0} \dfrac{r_c^*}{r_c}, & r_c > r_c^* \\ \rho_{d_0}, & r_c \leq r_c^* \end{cases} \quad (20)$$

Where, ρ_{d_0} is the initial droplet density before bloating, ρ_d is the droplet density during the decarburisation reaction, r_c is the decarburisation rate and r_c^* is the critical decarburisation rate, which is empirically correlated with the iron oxide concentration in the slag. The critical decarburisation rate (r_c^*) has been evaluated by the following empirical relationship.[37]

$$r_c^* = \begin{cases} 2.86 \times 10^{-4} \times 20, & wt\ pct\ FeO > 20 \\ 2.86 \times 10^{-4} \times (wt\ pct\ FeO), & wt\ pct\ FeO \leq 20 \end{cases} \#(21)$$

Assuming the droplets are spherical in shape, the following equations have been used to calculate the evolution of the surface area of a droplet as a function of residence time in the emulsion phase:

$$d_p(t) = \left(\frac{6}{\pi} \times \frac{m_d}{\rho_d(t)}\right)^{1/3} \quad (22)$$

$$A_d(t) = \pi \times d_p(t)^2 \quad (23)$$

where m_d is the mass of the ejected droplet and $d_p(t)$ and $\rho_d(t)$are the time varying diameter and density of droplet in the emulsion .

1.2.1.5 Size distribution of droplets

The size of ejected droplets can exert significant influence on reaction kinetics in the emulsion. [18] Therefore, a size distribution model was applied to calculate the diameter of droplets at the place of their birth from the bath. The model assumes that the size distribution of metal droplets follow Rosin-Rammler-Sperling (RRS) distribution function.[45, 46]

$$R_s = 100\, e^{\left[-\left(\frac{d}{d'}\right)^n\right]} \text{ in wt \%} \tag{24}$$

where R_s is the quantity of screen oversizes with diameter d. n and d' are parameters of distribution function, which represent homogeneity of distribution and the measure of fineness respectively.

The granules of metal droplets collected from the emulsion by Cicutti *et al.*[45] was found to vary between 2.3×10^{-4} m to 3.35×10^{-3} m. In this work, the similar droplet size spectrum has been used to determine the initial size distribution of ejected droplets. The total range of droplet size has been divided into ten classes with a mean diameter of d_p for each size class. The average diameter increment between two adjacent classes was taken to be 3.12×10^{-4} m. The proportion of droplet weight $W_{d,p}$ corresponds to class p, was obtained by applying the RRS distribution function as follows:

$$W_{d,p} = W_{d,total}\left(\exp[-\left(\frac{d_{p+1}}{d'}\right)^n - \exp[-\left(\frac{d_p}{d'}\right)^n\right) \tag{25}$$

Where $W_{d,\,total}$ is the total number of droplets ejected at a time interval of Δt which has been calculated by Eq. 26:

$$W_{d,total} = R_{B,T} \times \Delta t \quad (26)$$

Where $R_{B,T}$ is the modified droplet generation rate (kg/s), defined by author's previous work [45]:

$$\frac{R_{B,T}}{F_{G,T}} = \frac{\left(N_{B,T}\right)^{3.2}}{\left[2.6 \times 10^{6} + 2.0 \times 10^{-4}\left(N_{B,T}\right)^{12}\right]^{0.2}} \#(27)$$

Where $F_{G,T}$ and $N_{B,T}$ are the temperature corrected volumetric flow rate and modified blowing number respectively and $R_{B,T}$ is the amount of droplet generated per volume of gas. The detail calculation of temperature modified blowing number ($N_{B,T}$) and gas flow rate ($F_{G,T}$) can be found elsewhere.[47]

The parameters of the distribution function n and d' were chosen such a way that about 95% of the particles lie between 2.3×10^{-4} m to 3.35×10^{-3} m. By using the nonlinear least square fitting, the values of n and d' are estimated to be 1.75 and 1.26 respectively. The parameters in the RRS distribution function presented here may not be universal as the value of d', is a function of blowing conditions. [46,48] The present value of n falls in the same range (1.44±0.43) suggested by Subagyo *et al.* [48]

1.2.1.6 Residence time of the droplets

The mathematical model for the residence time of the metal droplets was based on the principle of ballistic motion, as proposed by Brooks *et al.*[32] The trajectory of a droplet in both vertical and horizontal direction was calculated by the force balance method with taking

into account the dynamic change in density under the influence of bloating. Thus, the decarburisation rate was coupled with the equation of motion to estimate the density change in the emulsion. In the present model, it has been assumed that the droplets are ejected into the emulsion with a certain angle with respect to the melt surface. The following force balance equations have been solved in a two dimensional coordinate (r,z) to determine the trajectory of a metal droplet:

Force balance along the vertical direction (z-axis):

$$\rho_d V_d \frac{du_z}{dt} = F_B - F_G - F_{D,z} - F_{A,z} \#(28$$)

Force balance along the horizontal direction (r-axis):

$$\rho_d V_d \frac{du_r}{dt} = -F_{D,r} - F_{A,r} \#(29$$)

where u_z and u_r are the velocity of the drop in z and r directions. The forces F_B, F_G, $F_{D,Z}$, $F_{A,Z}$ are buoyancy force, gravitational force, drag force and added mass force respectively. Assuming the droplets to be sphere of diameter d_p, the motion of the droplets can be described by the following differential equations:

$$\frac{du_z}{dt} = \frac{2(\rho_s - \rho_d)g}{\rho_s + 2\rho_d} - \frac{\rho_s C_{D,z} A_d}{(\rho_s + 2\rho_d)V_d} u_z^2 \#(30)$$

$$\frac{du_r}{dt} = -\frac{\rho_s C_{D,r} A_d}{(\rho_s + 2\rho_d)V_d} u_r^2 \#(31)$$

The drag coefficient $C_{D,z}$ and $C_{D,r}$ in both z and r direction are calculated as a function of Reynolds number.

The initial velocity at the place of birth of the droplet was calculated by applying energy conservation principle suggested by Subagyo *et al.*[49]:

$$\frac{E_{kd}}{E_{kg}} = 0.00143 N_{B,T}^{0.7} \#(32)$$

where E_{kd} is the total kinetic energy absorbed by the droplets by the blowing gas per unit time and E_{kg} is the amount of energy created by the blowing gas per time. The equation of motion of droplet in both horizontal and vertical directions described by Eqs. 29 to 31 with Eq. 20 and 21 have been solved simultaneously to determine the trajectory and residence time of the bloated droplets. The residence time model determines the total time the droplet resides in the emulsion as a function of initial size, ejection angle, initial velocity and the slag properties.

1.2.1.7 Temperature at metal drop-slag interface

During the oxygen blowing process, the metal droplets are ejected from a localized superheated zone underneath the oxygen jet. Doh *et al.*[50], by coupling chemical reaction of post-combustion with computational fluid dynamics, reported that the maximum temperature of the flame front (as a result of post-combustion reaction) is located near to the bath surface. Since the metal drops are ejected from the jet impact area, the temperature of the droplet interface is expected to experience higher temperature than the bulk melt. During the flight time of drops in the emulsion, a gradual decreasing in temperature can be expected due to heat dissipation to the surrounding. Since temperature exerts a significant effect on the mass transfer coefficient and the equilibrium concentration at the reaction interface, a model has been proposed to estimate the interfacial temperature of the metal droplet in slag. It was assumed that the metal droplets are rigid spheres and are more likely to exhibit hot spot temperature at the time of ejection. According to Chao[51], the surface temperature of a

spherical metal drop having an initial temperature, T_0 and a uniform temperature of T_∞, when enters inside the emulsion, can be calculated as:

$$T_{drop} = T_0 + \frac{T_0 - T_\infty}{1 + \beta} \tag{33}$$

$$\beta = \left(\frac{\lambda_m C_{p,m} \rho_m}{\lambda_s C_{p,s} \rho_s}\right)^{1/2} \tag{34}$$

where λ is the conductivity (W/mK), C_p is the heat capacity (J/kg). The subscript m, s corresponds to hot metal and slag. T_{drop}, T_0 and T_∞ represents the temperature at the droplet interface in the emulsion, temperature of the droplet at the time of ejection and the emulsion temperature respectively.

Here we assumed $T_0 = T_{iz}$ and $T_\infty = Ts$ for the calculation of the temperature at the droplet interface. The heat capacity of the slag was calculated by the weighted average of the heat capacity of the individual oxide species in the slag.

$$C_{p,s} = \sum_{i=1}^{n} y_i C_{p,i} \tag{35}$$

Where y_i is the wt pct and $C_{p,i}$ is the heat capacity of oxides in the slag. The values of thermal conductivity and heat capacity of steel and slag used for this model are given in Table 4.

1.2.2 Macrokinetics- Estimation of total refining rate by the emulsion

The difference between the total weight of impurities (C, Si, Mn and P) ejected into the emulsion and returning to the bath, as represented by Eq. 7, was calculated at each time step to determine the overall refining rate by the emulsion zone. The total weight of impurities in the ejected metal droplets in the time step, Δt was determined by estimating the droplet

generation rate and the bath concentration as presented in Eq. 8 (Table 2). The total mass of impurities (in the droplets) returns to the bath at time t, was calculated from the refined concentration, a number of droplets, the weight of droplet and residence time for all the size groups, described by Eq. 9 (Table 2). The number of droplets returning to the bath for a particular size class was calculated from the proportional weight and average size of the droplets in the same size class. In a particular group, a uniform droplet size of all the ejecting droplets was assumed in the model calculation.

1.3. Slag-bulk metal zone

Due to the impact force of the top gas jet, the slag formed in the jet impact is likely to be pushed outwardly from the cavity and a region of permanent contact between the slag and metal can establish in the region near to the refractory wall of the vessel. This region was considered as slag-bulk metal zone and the impurities in the hot metal react with the slag to form their respective oxides. The condition of mixed controlled mass transfer was applied to estimate the reaction kinetics at the slag-bulk metal interface. Overall mass transfer coefficient was determined by Eq. 18. Similar to the jet impact zone, the mass transfer coefficient in the metal phase was calculated by using the correlation suggested by Kitamura *et al.*[23] as a function of bath geometry, temperature and stirring energy. The slag side mass transfer coefficient was determined as a function of stirring power and temperature. [7] The mathematical expressions for the mass transfer correlations are presented in Appendix A.1.

The area of slag metal (A_{sm}) interface was calculated by subtracting the cavity area from the geometrical area of the bath surface. For non-coalescence cavities, the area of slag-bulk metal interface can be expressed by the following equation:

$$A_{sm} = \pi\left(\frac{D_b^2}{4} - n_n \times r_{cav}^2\right) \tag{36}$$

Here D_b is the diameter of the bath surface (m), n_n is the number of nozzles in the lance tip and r_{cav} is the radius of the jet cavity (m).

In this study, the effect of surface oscillation was neglected in the calculation of the interfacial area between slag and bulk metal. The instantaneous equilibrium between the reactants and products was assumed at each computational time step and the interfacial concentration was determined from the partition ratio correlations described for slag-metal drop interface Table 3. The temperature and the concentration of bulk metal instead of metal droplet were applied in evaluating the interfacial concentration at the slag-bulk metal phase boundary.

1.4. Dynamic slag generation model

The rate equations for C, Si, Mn and P described in Table 2 need the dynamic input of slag oxide compositions to evaluate the kinetic parameters such as interfacial concentration and residence time of metal drops in the emulsion phase. A dynamic slag generation model was coupled with the multi-zone kinetic model for simultaneous estimation of slag and hot metal composition during the blow. Modeling of lime and dolomite dissolution was developed as a function of temperature, slag composition and stirring intensity as proposed by Dogan *et al.*[55] The saturation concentration of CaO and MgO was calculated as a function of slag composition and temperature using Factsage 7.1[56] thermodynamic package and were given as dynamic input to the model.

1.4.1 Fe_tO generation model

The Fe_tO generation model was developed by the method of oxygen balance inside the converter.[7] It was assumed that every mole of oxygen injected into the converter consumed by the chemical reactions. The difference between the mass of oxygen input and the oxygen consumed by oxidation of Si, Mn, P, C and CO, was used to calculate the oxygen available

for iron oxide formation in slag. The weight of oxygen injected into the furnace via top blowing and the oxygen contained in the iron ore was considered as model inputs. Oxygen consumption by C, Si, Mn, P and CO was evaluated from the kinetic models at each time step. **Figure 4** shows the schematic of dynamic Fe_tO calculation in slag by the method of oxygen balance. A fixed ratio of FeO/Fe_2O_3 = 0.3 was considered at the slag and hot metal phase boundary.[57] The total iron oxide (%Fe_tO) in slag, at a given time step, was estimated from the avilable oxygen (kg) and the slag weight. The weight of slag was calculated by adding individual oxide components in slag, generated from oxidation reactions and dissolved flux at each computational time step.

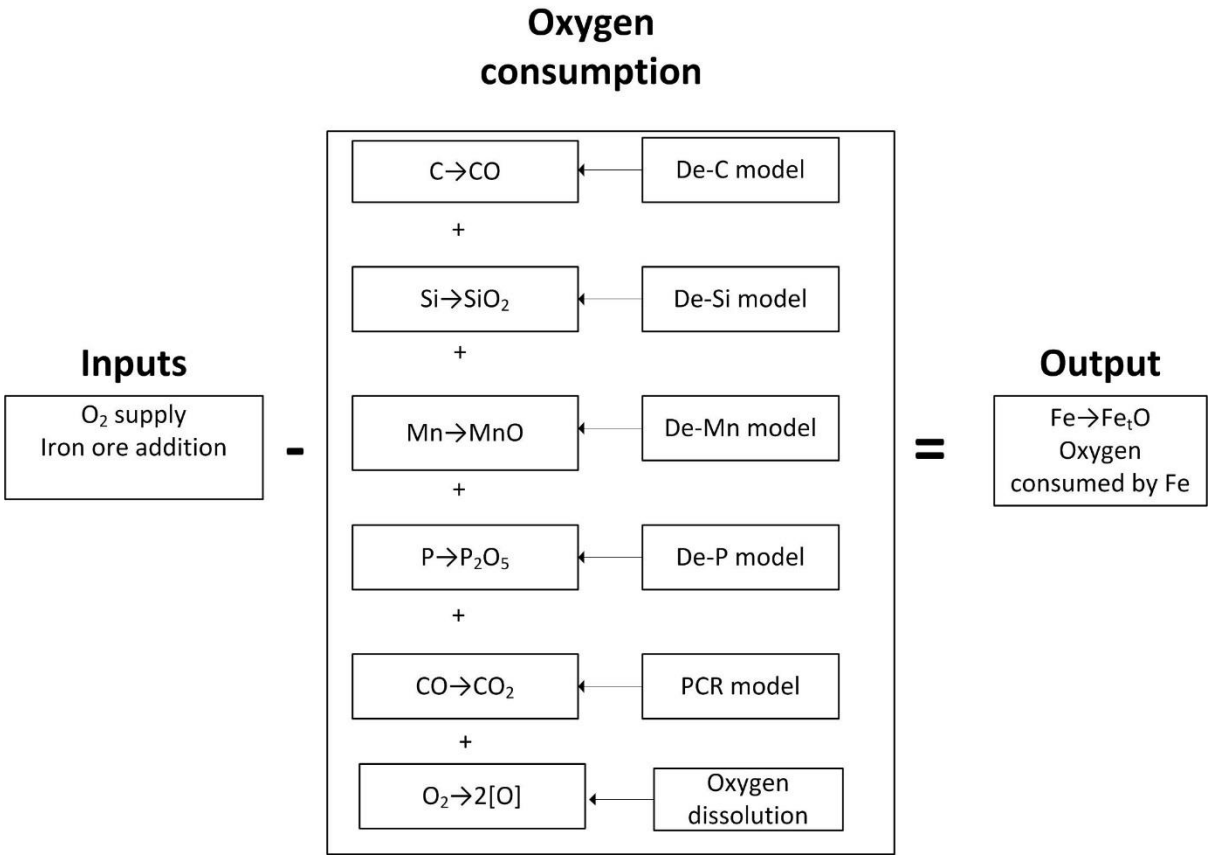

Figure 4: Model for Fe_tO evolution during blowing period

The oxygen mass balance equation for the calculation of iron oxide concentration in slag can be expressed by the following equation:

$$0.01 \times \frac{16}{71.5} \times W_s^t \times \frac{d(\%FeO)}{dt} = \left(\frac{dW_{O_2}}{dt} + \frac{48}{159.7} \times \frac{dW_{ore}}{dt}\right) - 0.01 \times \frac{16}{12} W_m^t \times (1 - PCR) \times \frac{d[\%C]}{dt} - 0.01 \times \frac{16}{12} W_m^t \times PCR \times \frac{d[\%C]}{dt} - 0.01 \times \frac{32}{28} W_m^t \times \frac{d[\%Si]}{dt} - 0.01 \times \frac{16}{55} W_m^t \times \frac{d[\%Mn]}{dt} - 0.01 \times \frac{80}{62} W_m^t \times \frac{d[\%P]}{dt} - 0.01 \times W_m^t \times \frac{d[\%O]_b}{dt} \quad (37)$$

where W_{O2} is the weight of injected oxygen, W_{ore} is the weight of ore and PCR denotes the post combustion ratio. W^t_m and W^t_s are the hot metal and slag weight respectively, expressed by Eq. 38 and 39.

$$W_m^t = W_m^{t-\Delta t} - \Delta W_{m,ref}^t + \left(\frac{dW_{sc}^m}{dt}\right)\Delta t + \frac{2M_{Fe}}{M_{Fe_2O_3}}\left(\frac{dW_{ore}}{dt}\right)\Delta t \quad (38)$$

$$W_s^t = W_s^{t-\Delta t} + \Delta W_{MOx} + \left(\frac{dW_L}{dt}\right)\Delta t + \left(\frac{dW_D}{dt}\right)\Delta t \quad (39)$$

Where, $\Delta W_{m,ref}^t$ is the weight of refined hot metal, $\frac{dW_{sc}^m}{dt}$ is the scrap melting rate, M_{Fe} and $M_{Fe_2O_3}$ are the molar mass of iron and iron (III) oxide. In Eq. 39, ΔW_{MOx} is the sum of all the oxide, $\frac{dW_L}{dt}$ and $\frac{dW_D}{dt}$ are the dissolution rate of lime and dolomite respectively.

In the above calculation, it was assumed that the top gas contains 100% oxygen and the iron ore was considered to be pure hematite (Fe_2O_3). The dissolved oxygen concentration in the bulk metal has been calculated from the equilibrium value with the slag ((FeO) = [Fe] +[O]).

1.5. Post-combustion

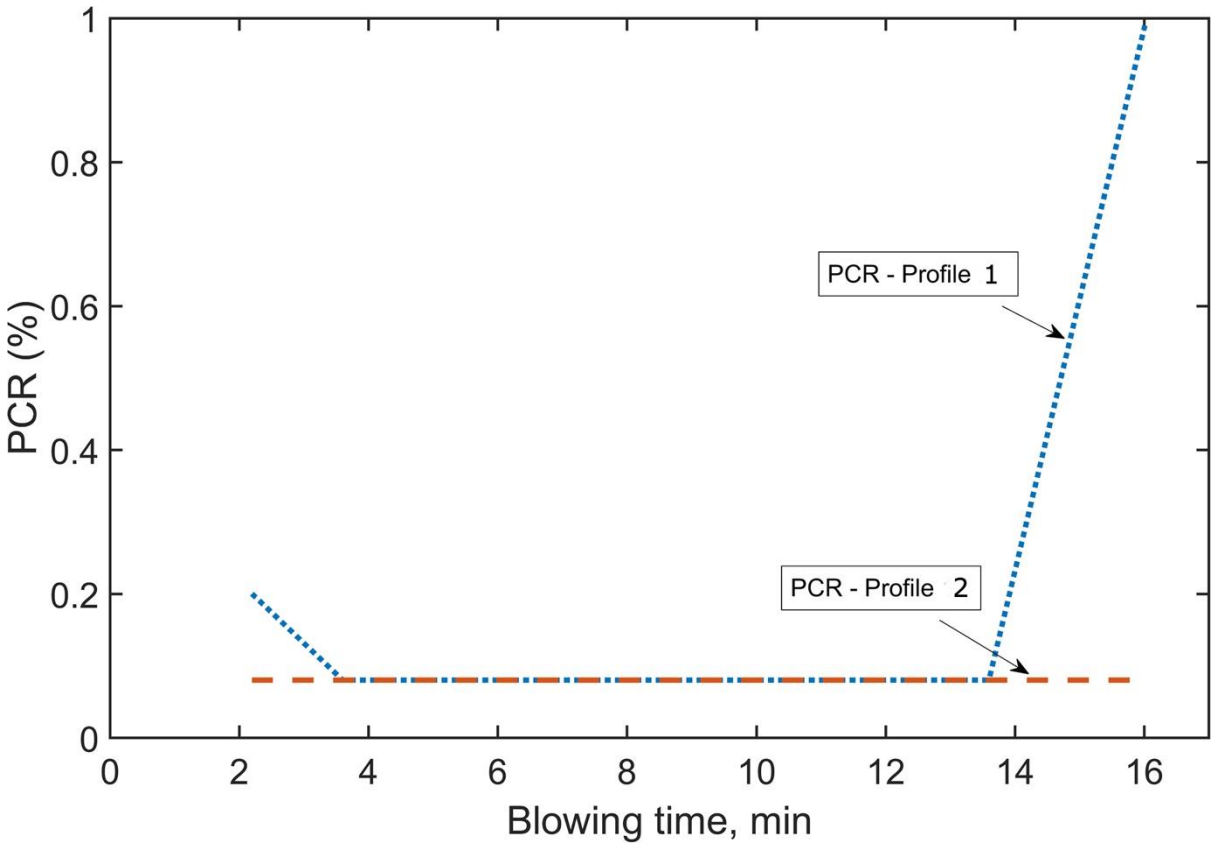

Figure 5: Post-combustion profile used for Fe_tO generation model. PCR- (post-combustion ratio)

As can be seen from Eq. 37, the estimation of wt pct Fe_tO in the slag needs the quantitative information of how much oxygen consumed by CO to form CO_2. It has been observed that the mechanism of post-combustion in the converter is complex, resulting from heterogeneous chemical reactions occurring in the unsteady state. The dynamic process variables like the change in lance height, scrap characteristics, oxygen flow rate and the height of slag foaming exert a substantial effect on the post-combustion ratio.[58]These variables change rapidly particularly during the initial stage of blowing. Due to the above complexity, a simplified approach was considered in order to investigate the effect of post-combustion on Fe_tO evolution during the blowing process. Two profiles of post combustion ratio (PCR), based on the observed plant data were considered in the model calculations. In profile 1, a dynamic PCR profile in which the concentration CO was assumed to change linearly during 0 to 20%

and 80 to 100% of blowing time.[59] In profile 2, a constant PCR value of 0.08 was taken throughout the blow. The two different PCR profile employed in the model calculations are illustrated in **Fig. 5.**

2. Computation model development

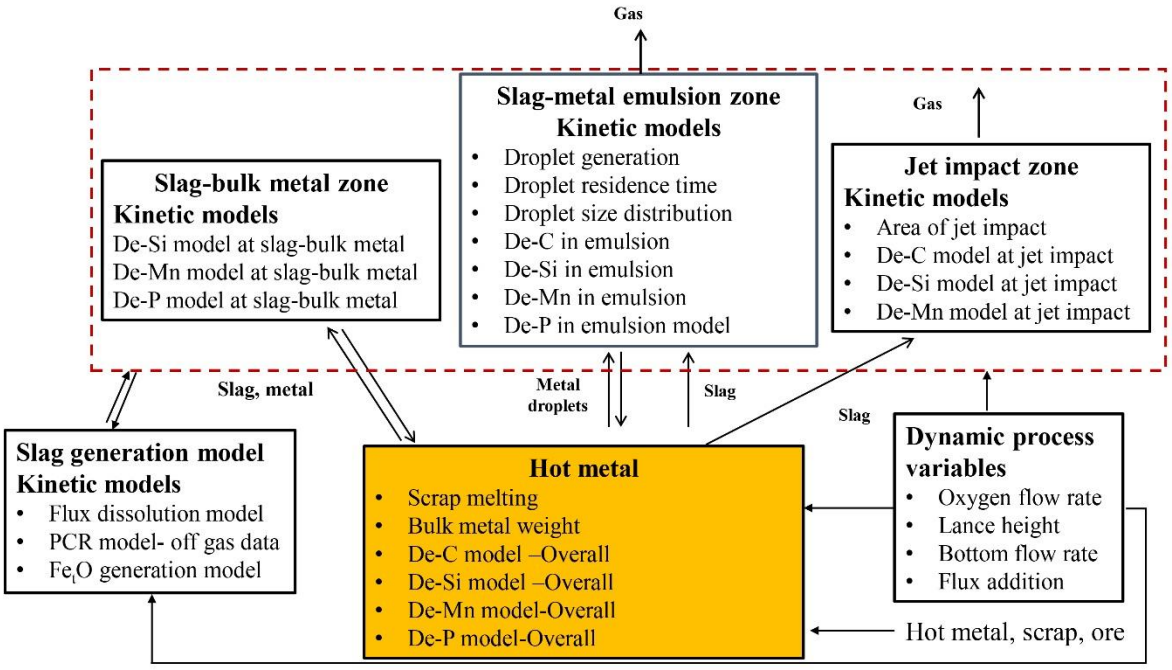

Figure 6: A three zone kinetic model for prediction of metal and slag composition during blowing period of a top/combined blowing steelmaking converter process

For better representation of overall process model and interaction between various phases, the system has been divided into three reaction zones and several sub-models are developed to estimate the thermodynamic and kinetic parameters of refining reactions in each zone. **Figure 6** illustrates the schematic of the three reaction zones and the sub-models in each zone. The reaction zones are connected each other by material and heat flow. Metal and slag transfer takes place at jet impact and slag-bulk metal boundary whereas metal drops and slag transfer takes place between the emulsion and hot metal. The mass flows such as hot metal, scrap, and iron ore are given as input to the hot metal reaction zone. The dynamic parameters such as oxygen flow rate, lance height, bottom blowing rate, and flux addition were given as input to

522 the sub-models in each reaction zone. Each submodel is built separately and finally connected
523 each other to simulate the overall process. For example, a droplet generation model was built
524 separately and connected with micro-kinetic model for the droplet to estimate the total rate of
525 refining in emulsion zone.

526 **2.1. Assumptions**

527 The following assumptions were taken during the formulations of the dynamic model.

528 1. The reactions in the BOF were confined to three primary regions. The possibility of
529 several other reactions such as between the refractory material and slag/metal, reverse
530 emulsification (slag drops inside bulk metal) were ignored in this study.
531 2. A heat balance model to calculate the temperature of metal and slag has not been
532 included in this study. A linear temperature profile, which varies between 1623K
533 (1350 °C) to 1923K (1650 °C) during the blowing period, was used for the calculation
534 of hot metal temperature. The slag temperature was considered 100 °C higher than the
535 hot metal temperature. [5] The authors are aware that a linear temperature profile is
536 simplified assumption, may be ideally suited for the Cicutti's heat data (measured
537 bath temperature varies linearly during the blow). However, in real steelmaking
538 practice, the type and amount of scrap or flux addition practice can have a significant
539 impact on the thermal profile of hot metal, which need to be taken into account in the
540 dynamic model.
541 3. It was assumed that 30 ton of scrap had been melted entirely during first 7 minutes of
542 the blow. A linear scrap dissolution rate, based on the model result by Dogan *et al.*[5]
543 was used. The linear melting rate assumption may not be necessarily correct since the
544 melting (and dissolution) of scrap proceeds with the formation of solidified pig iron
545 layer on the top at the beginning period and it delays the melting process. In the

present work, a simplified assumption of rapid melting of the shell is considered to demonstrate the general principle of the multi-zone kinetic model in a BOF process.

4. Iron ore was charged into the furnace during the initial stage of furnace operation. It was assumed that the dissolution of iron ore completes during the first 2 minutes of the blow.
5. The lime and dolomite particles added into the furnace are assumed spherical having diameter 0.045 m and 0.03 m respectively. One ton of lime and 1.7 ton of dolomite were added before the start of the blow. The remaining amount of lime was added in a continuous interval within 7 minutes of the blow. The remaining dolomite was added 7 min after the start of the blow.
6. The droplets ejected from the melt were assumed as spherical in shape. The angle of inclination of the droplets is assumed 60° with respect to the bath surface. In a practical BOF operation, a small fraction of metal fragments are escaped from the mouth of the converter and some are caught by the jet and return to the melt phase. However, in the present model, it was assumed that all the droplets ejected from the melt participate in the reactions in the emulsion zone. The effect of bottom flow rate on droplet generation was ignored in this study.
7. While discretizing the continuous process of droplet generation, it was assumed that all the droplets in a given time step Δt are ejected simultaneously at the start of each computational step.
8. The motion of metal droplets in the emulsion is influenced by the density and viscosity of the slag-gas continuum. Ito and Fruehan reported that the gas volume fraction in the emulsion varies from 0.7 to 0.9. [60] The average value of 0.8 has been adopted in the model.

2.2. Computational strategy

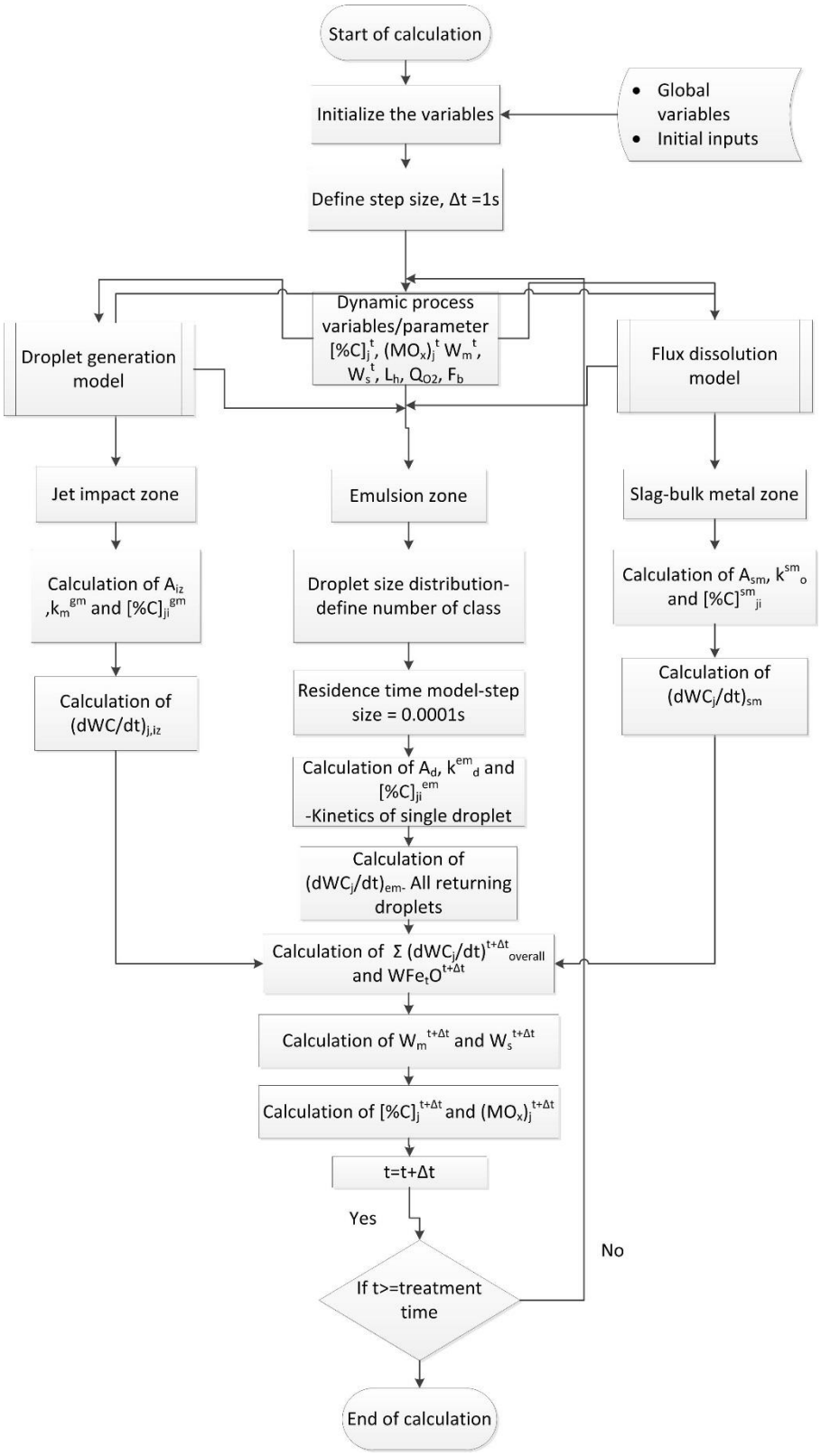

Figure 7: Algorithm for BOF dynamic model

The numerical program uses explicit finite difference method, which marches forward with time, solving for the bath and slag composition at next time step by using the input parameters calculated in the previous time step. The solution starts at the second time step based on the initial conditions, which were given as an input to the model. The computational platform uses a central model where the calculation of liquid metal concentration, slag composition, slag weight and hot metal weight takes place and several sub-models to evaluate the transient rate parameters. The central model has been connected in parallel with the sub-models.

Figure 7 demonstrates the flowchart of the computation program of the complete mathematical model. Initially, the value of the global parameters such as constants, properties of slag and metal (e.g., density, molecular weight) were given as input to the model. At the start of the program, the parameters such as slag compositions, metal chemistry, hot metal weight, slag weight, the temperature of metal and slag have been given as initial input to the computational program.

The simulation starts after 2.2 minutes of the blow, as the data of slag and metal became available after this time. Once, the step size was selected, the dynamic process variables such as lance height, oxygen flow rate, bottom blowing flow rate were given as input to the model at each time step by predefined functions obtained from converter operation. The flux dissolution models compute the amount of lime and dolomite dissolved in slag at each time based on the dynamic flux addition inputs. The amount of droplet generated from the melt was calculated by the modified droplet generation sub-model and has been used to estimate the total refining by the emulsion zone. In the emulsion zone, a time step of 0.0001s was chosen to calculate the trajectory of metal drops. The rate of refining of hot metal from the different zones was computed at each time step. The overall rate of C, Si, Mn and P in the

previous time step was used to calculate the weight of iron oxide (W_{FeO}) generated at each blowing time. The weight of slag evolution at each time step was evaluated by summing all the oxides of Si, Mn, P and Fe with the dissolved amount of flux. Once the weight of metal and slag are known, mass balance is performed to predict the wt pct of metal and slag composition at t+Δt. The calculation continues until the time reaches the total blowing time of BOF operation.

2.3. Input data

The initial input and the process parameters used for the model were taken from a 200-ton LD converter studied by Cicutti *et al*.[45] Table 5 shows the complete list of parameters used to develop the model. The metal and slag sample in their work was collected from the mouth of the converter by use of a special sampling device. The initial value of slag and metal compositions were taken as the input to the model. The measured slag and metal composition at different intervals of blowing time were used to validate of the model predictions. The blowing profiles (both top and bottom) employed in the converter operation were given as dynamic input to the model. The other parameters used for calculating the physicochemical properties of slag, metal and gas are listed in Table 5.

2.4. Steady state solution

To establish the optimal solution, a mathematical convergence analysis was performed for different iterative time steps. Numerical stability of the solution is reached when the solutions for various time steps are converged. **Figure 8** shows the predicted value of carbon concentration in the bath as a function of blowing time for the different value of computation time. The time step (Δt) was varied from 0.5 to 10 second and the decarburisation profile was produced for each time step. As can be seen from **Fig. 8,** when the time step becomes smaller, the solution for 0.5 and 1s was identical, which proves the computational accuracy of the computer program. To reduce the computational time, the time step of 1 s was selected in

the present model calculations. The total computation time for the dynamic slag and metal prediction for one blowing period using Matlab© 2016a on a Windows PC has Intel(R) Core(TM) i5-4570 CPU @3.20GHz with 8GB RAM is approximately 20 minutes.

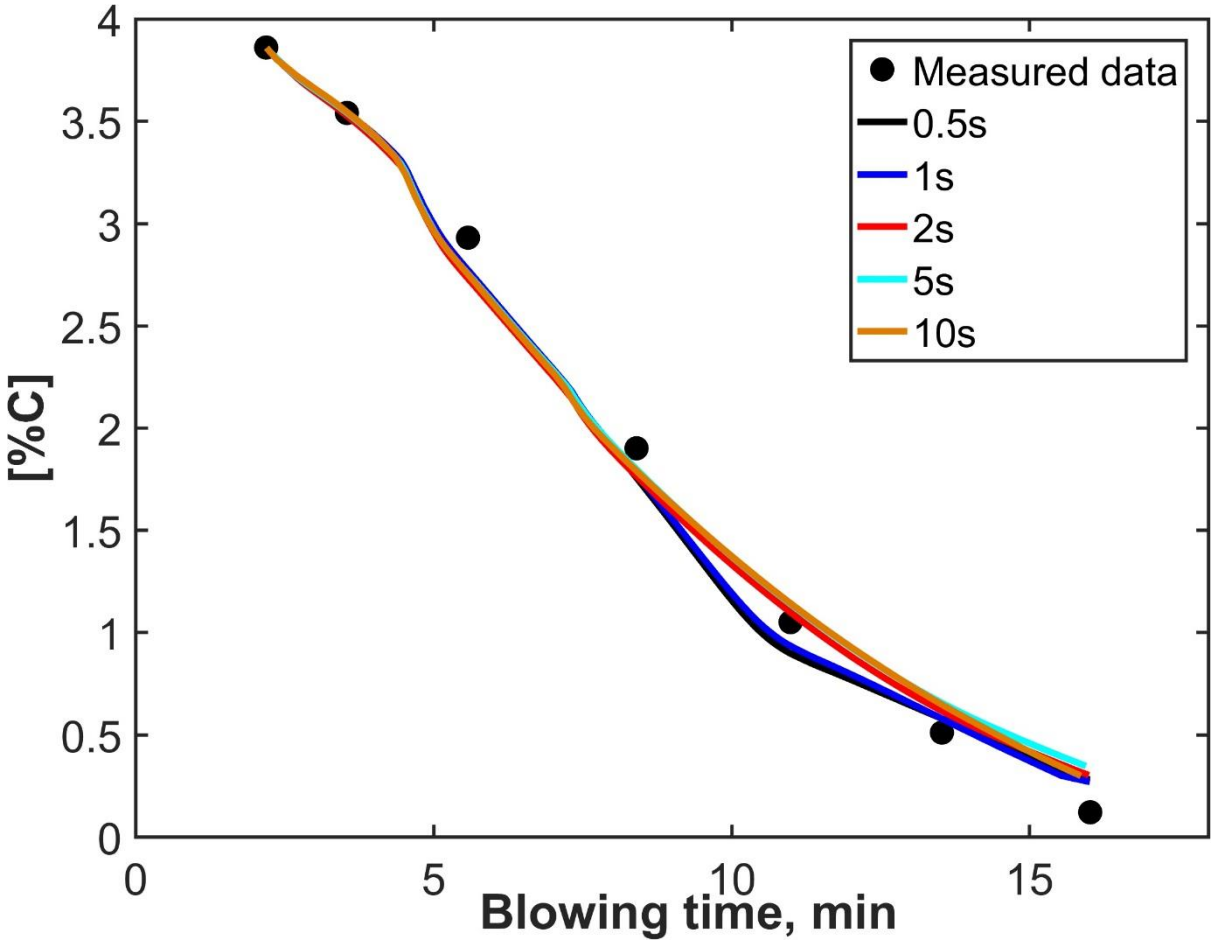

Figure 8: Model prediction of carbon concentration variation as a function of blowing time with different computational time steps

3. Model validation and discussions

3.1. Temperature at the reaction interfaces

A thermal gradient can exist inside a BOF converter due to the formation of localized reaction zones. Numerous researchers attempted to measure the temperature at different zones of the converter.[63, 64] Chiba *et al.*[63] reported that the temperature of the hot spot jumps suddenly to 2273 K (2000 °C) at the beginning stage of the blowing, then fluctuates

between 2373 K (2100 °C) to 2773 K (2500 °C) during the main blow period and finally equals to the hot metal temperature. Rote and Flinn observed that the temperature difference between the top surface and bottom of the vessel varies between 200 and 400 K depending on the blowing type (soft or hard blowing).[64] Since the temperature is an essential factor in the equilibrium partitioning of refining elements, the model calculations for interfacial temperature in different reaction zones were developed.

In common with Chiba *et al.*, it was assumed the temperature in the hot spot increases linearly from 2273 K (2000 °C) to 2573 K (2300 °C) during the first 25% of the blow. During the main blow, between 25 to 80 % of the blow, the temperature was maintained at a constant value of 2573 K (2300 °C). Finally, the temperature gradient between the hot spot and the liquid bath begins to disappear and hot spot temperature gradually decreases after 80% of the blow.[65] Industrial measurements indicated that the temperature of slag is generally 20 to 100 K hotter than the hot metal during the blowing period.[66] The temperature difference between the metal and slag was reported to be high during the initial period and the gradient becomes smaller towards the end blow period. In the present work, for the sake of simplicity, the average temperature of the slag was assumed to be 100 K higher than the hot metal temperature.

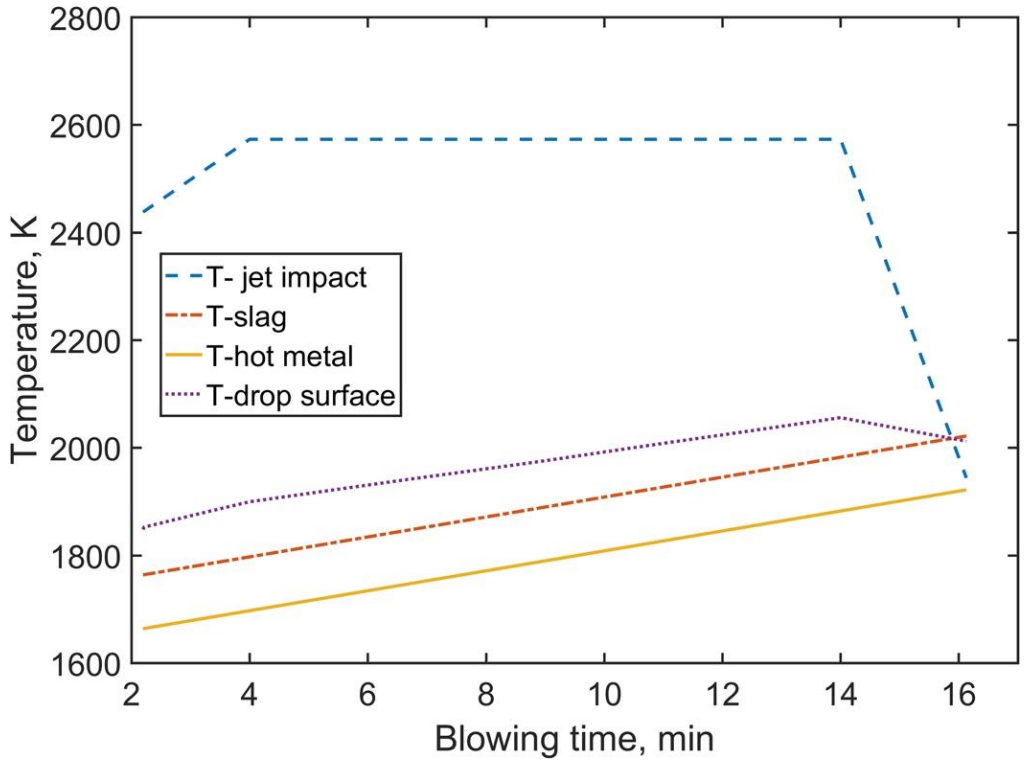

Figure 9: Temperature change across various reaction interfaces inside the furnace during the blowing time

The surface temperature of the moving droplets in the slag-metal emulsion was calculated by applying Eq. 33. The variation of temperature in different zones of the converter used in the model is shown in **Fig. 9**. It was observed that the surface temperature of the droplets is 90 to 200 K higher than the metal bath temperature. The temperature profile of droplet surface varies linearly with the blowing time during almost all the part of the blow. Toward the end of the blow, there is a decreasing trend observed which is due to a reduction in the hot spot temperature as a result of slowing down of the decarburization reaction. It should be acknowledged that the current procedure for estimation of interfacial temperature is based on several simple assumptions and no rigorous heat balance model was applied in the calculation. A dynamic heat balance model focusing the micro and macrokinetics of heat transfer in the recirculated metal drops in the emulsion, coupled with the present multi-zone model can provide a clear insight of reactions in a BOF process.

3.2. Kinetics of refining of droplet in the emulsion

The model predictions of the compositional change of two classes of droplets having average diameter 6×10^{-4} m (0.6 mm) and 9×10^{-4} m (0.9 mm) at 2.5^{th} minutes of blowing time are shown in **Fig. 10**. The reaction rate of Si, Mn and P in the droplet are found to be rapid and reaches the state of equilibrium within a few seconds in the emulsion. In the 0.6 mm droplets, the concentration of Si, Mn and P approaches its equilibrium value within 2 seconds. In contrast, the refining of C continues during the entire 27 seconds of residence in the emulsion phase. It was also observed that the refining rate of droplets, particularly decarburisation is a function of droplet size. The droplets in the lower region of size spectrum exhibit high efficiency of refining and make a greater contribution to the conversion process of Si, C, Mn and P during the reaction in the emulsion. About ~60% of decarburization was observed for 0.6 mm droplet in contrast to ~18% when the droplet size was increased by 0.3 mm. The may be due to a shorter reaction time (~10 s) of 0.9 mm diameter droplet as compared to 0.6 mm droplets (~27 s). Here the extend of decarburisation reaction is limited by the time of reside of droplet in emulsion. The model prediction of the droplet refining kinetics has been found to be consistent with the observed refining of metal drops reported by IMPHOS pilot plant experiments.[18] The measurements of droplet composition collected from the emulsion sample shows a high depletion of Mn, P and Si but the C concentration is more than 1 wt pct during the initial blowing period. The rapid removal rate of Si, Mn, and P during the opening stage of oxygen blow is thought to be the result of high thermodynamic driving force and large surface area created by small size metal drops in the emulsion.

687 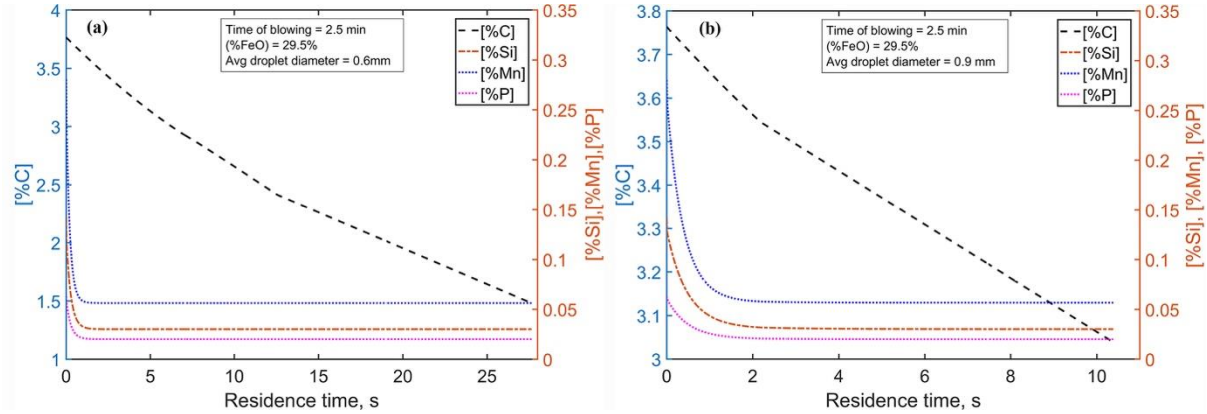

688 Figure 10: Removal kinetics of C, Si, Mn and P of a single metal drop in emulsion (a) Initial
689 droplet diameter = $6x10^{-4}$ m (b) Initial droplet diameter = $9x10^{-4}$ m

690 **3.3. Validation**

691 The variation of bath concentration was simulated by the three zone kinetic model with the
692 dynamic change of process variables for a 200 ton LD-LBE converter. **Figure 11** illustrates
693 the simulated profile of C, Si, Mn and P as a function of blowing time for the predefined PCR
694 profiles. As can be seen from the figure, the model predictions of bath composition with PCR
695 profile 1 agree well with the measured solute concentrration during different intervals of the
696 blowing period. It was observed that changing the post combustion ratio does not have much
697 influence on the predictions of C and Si, albeit the reversion behaviour of Mn and P are
698 highly influenced by post combustion ratio. This is most likely due to the strong dependence
699 of the equilibrium concentration of Mn and P on the change of slag chemistry (slag Fe_tO),
700 which in turn is controlled by the amount of oxygen consumed in the process of post-
701 combustion reaction.

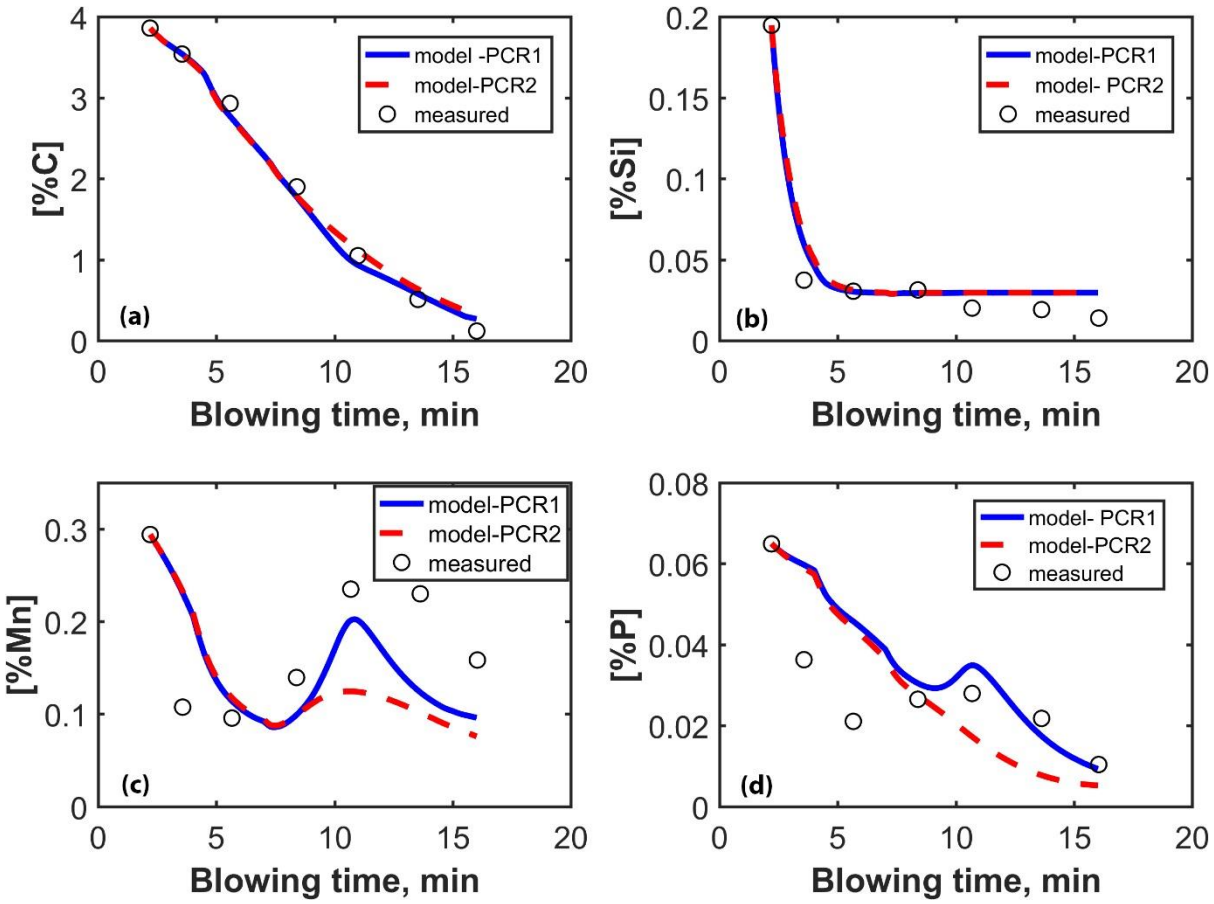

Figure 11: Model prediction of hot metal composition (wt pct) during the blowing period. (a) Carbon, (b) Silicon, (c) Manganese, (d) Phosphorus

The model prediction of decarburization has been found to be in excellent agreement with the plant data. The three distinct region of decarburization profile, commonly observed in a BOF process, was distinguished in the model prediction. The Si refining predicted by the model was found to be consistent with the measured values. As reported in the previous publication, the refining of Si can be explained by a three-zone approach where a significant fraction of refining is observed to take place by the droplets mechanism.[27] In the case of Mn removal, the high rate at the beginning of the blow, reversion during the middle of the blow and again increase in rate towards the end blow was captured by the model. It was observed that the oxidation and reversion of Mn from slag to metal is primarily caused by the droplet recirculation by the emulsion zone. The equilibrium concentration of Mn at the metal drop-slag interface, which is strongly dependent on temperature and slag chemistry, was found to

716 be the deciding factors for reversion of Mn. The details about the mechanism of Mn refining
717 and the role of different reaction zones on the rate will be discussed separately.[21] The rate of
718 P refining predicted by the model shows a similar oxidation and reversion behaviour as Mn.
719 The reversion of P predicted by the model shows a similar behaviour as the actual process.
720 However, a slow removal rate of P as compared to the actual process was noticed. The
721 mismatch between the Mn and P predictions may be caused by the error in evaluation of rate
722 parameters and estimation of equilibrium concentration at the metal drop and slag interface.
723 An increase in slag-bulk metal interfacial area as a result of surface oscillation could be
724 another reason for the deviation. Further experimental work of the reaction kinetic study of
725 Fe-C-Si-Mn-P drops in steelmaking slag is essential to evaluate the kinetic parameters
726 associated with the simultaneous oxidation/reduction reactions.

727 The evolution of slag during the blowing process for the predefined two post-combustion
728 profiles are illustrated in **Fig. 12**, and the results are compared with the measured slag data.
729 As can be seen from the figure, the concentration of oxides in the slag is in consistency with
730 the measured values in both the PCR profiles. However, it can be noticed that the level of
731 Fe_tO is sensitive to the oxygen consumed by post combustion reaction. The PCR profile 1
732 where a dynamic post-combustion ratio was adopted has been found to produce better results
733 for Fe_tO prediction than a constant PCR. During the initial part of the blow, i.e. after one
734 minute from the start of computation, the weight of Fe_tO was found to increase with time. It
735 might be due to the slow decarburization rate and Fe_tO was not consumed entirely during the
736 initial stage. After approximately 5 minutes of the start of the blow, the Fe_tO percentage starts
737 to decrease because the rapid rate of decarburization begins to take place and Fe_tO was
738 largely consumed by carbon. Until 10 min or so, Fe_tO reaches the lowest value and after that,
739 it increases due to decreasing in hot metal weight in the emulsion phase. This results in
740 slowing down the Fe_tO consumption rate by the droplets. A deviation of Fe_tO between the

model and the measured value was observed during the end blow period. In the present calculation of Fe_tO, when the impurity level reaches to the low level, virtually all the injected oxygen ends up in forming iron oxide and thus a sharp rise in slag iron oxide was observed. The kinetics of Fe_tO formation with regard to saturation of Fe_tO (the equilibrium driving force of FeO between the bulk and interface) in slag and the loss of Fe as dust was not considered in the present work. Also an inaccuracy in post combustion ratio may introduce some error in oxygen balance equation. The above factors may be responsible for the deviation observed in the simulated iron oxide profile, particularly during initial and end blow period. Due to the overestimation of Fe_tO in the end blow period, the model prediction of slag weight and CaO concentration finds some deviation from the measured values.

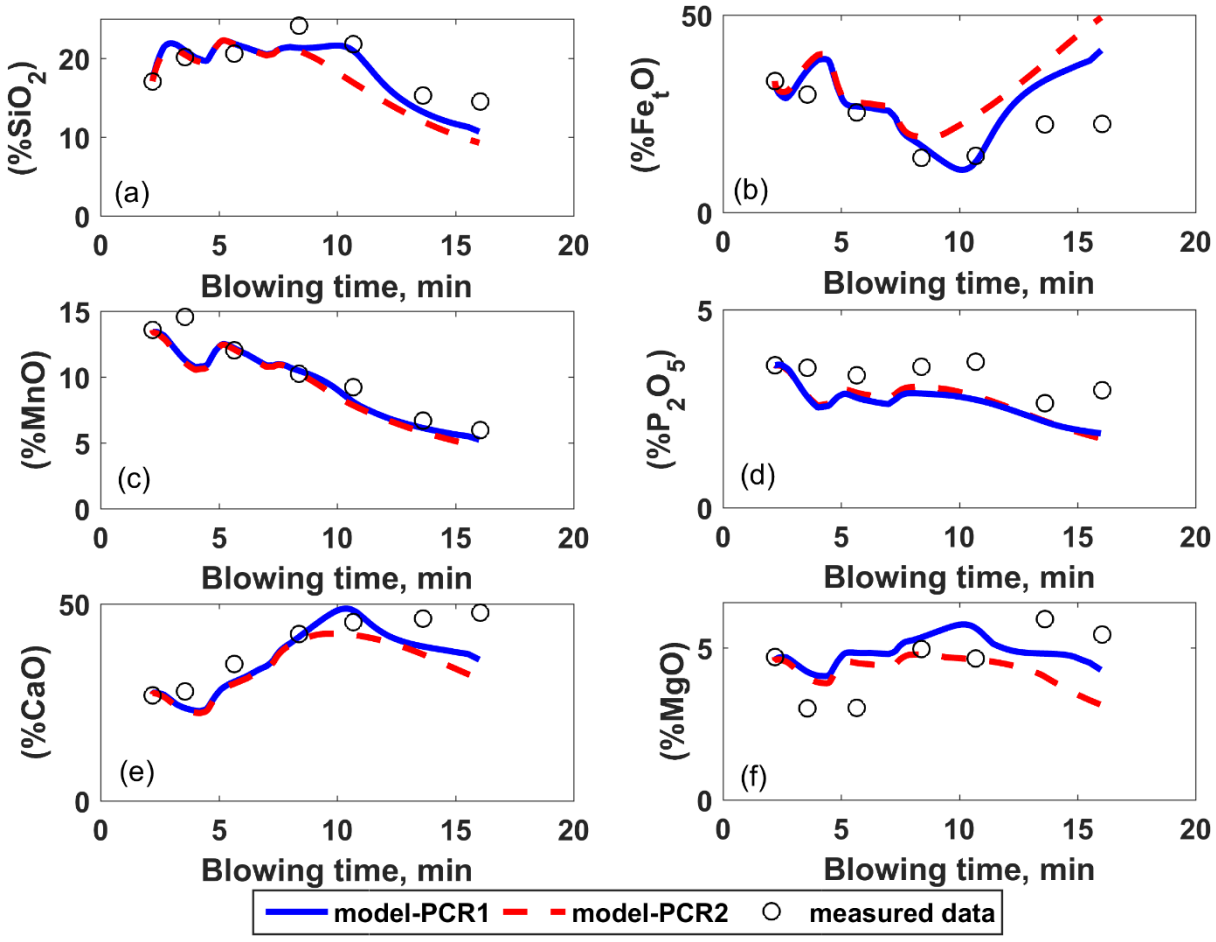

Figure 12: Evolution of slag composition (wt pct) during blowing period. (a) SiO_2, (b) Fe_tO, (c) MnO, (d) P_2O_5, (e) CaO, (f) MgO.

The evolution of hot metal weight and the slag during the blowing period for PCR 1 profile is shown in **Fig. 13**. The change in the weight of the melt is calculated using the amount of scrap melted, the amount of droplet generated and fall back and the weight of metal loss by forming slag during time step Δt. It can be observed that the weight of the hot metal increases gradually due to the gradual melting of the scrap until 7 minutes of the blow. After this period, the bulk metal weight decreases till the end of blow due to oxidation loss of various impurities from the melt. Similarly, the weight of slag increases initially due to the dissolution of lime and dolomite continuously. The deviation of slag weight after 10 minutes of the blow is due to the overestimation of Fe_tO calculated by the model.

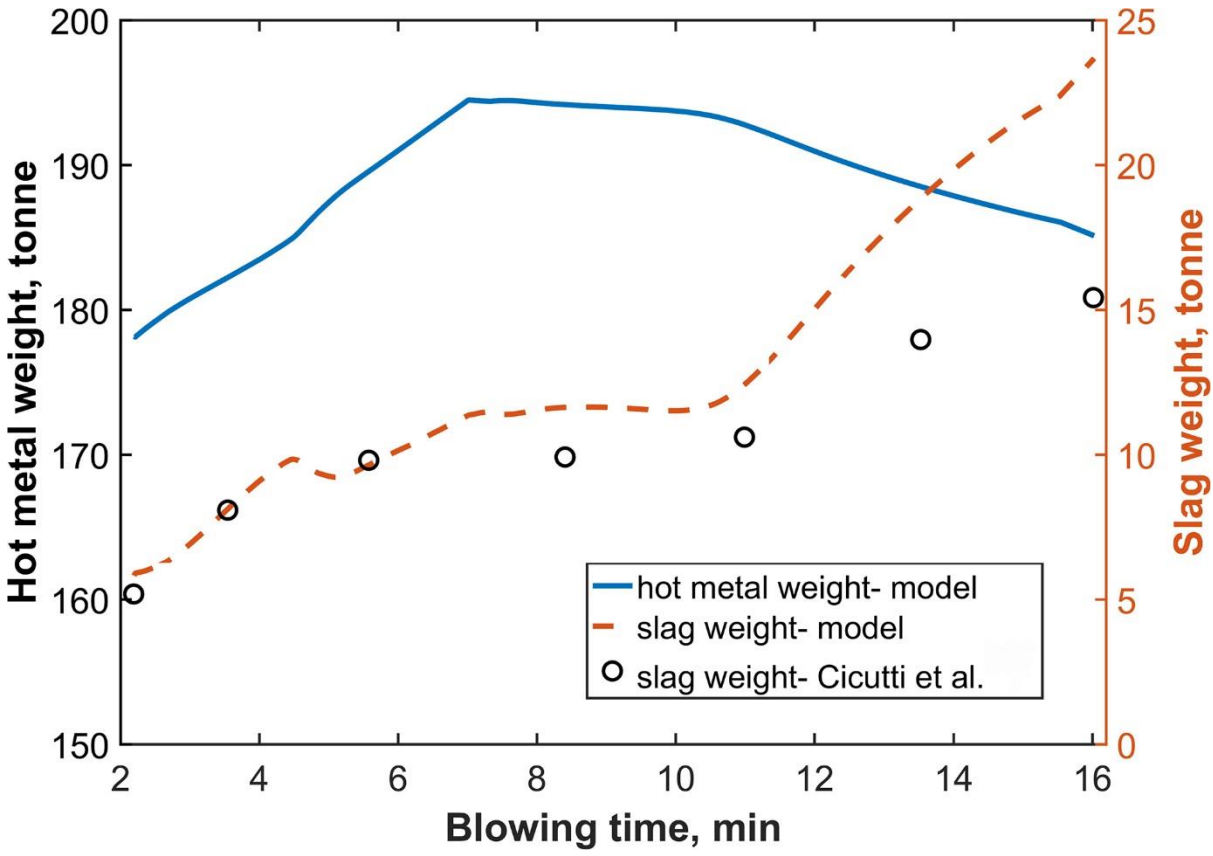

Figure 13: Variation of hot metal and slag weight during the blowing period as predicted by the model for PCR profile 1

It should be acknowledged that the current study does not include the effect of bottom blowing on droplet generation. While there is evidence that bottom blowing affects the

droplet generation rate in a combined blowing converter, none of the predictive models yet incorporated the bottom blowing effect on the estimation of the droplet generation rate in oxygen steelmaking process. Due to unavailability of quantified models, the authors have ignored the effect of bottom blowing in the present work.

4. Conclusions

A three-zone kinetic model has been developed to predict the metal and slag compositions during the BOF process. The converter was divided into three reaction zones and kinetics of refining in each zone has been estimated by providing mathematical treatment to the physicochemical process occurring in different zones of the converter. The fundamental understanding of BOF process such as bloating and refining of metal droplets in the slag-metal emulsion, the reaction taking place in the jet impact zone and slag-bulk metal region were successfully incorporated into the mathematical model. A Fe_tO generation model was developed and coupled with the kinetic model for simultaneous prediction of slag and metal during the blowing process. The following conclusion can be made based on the present study.

1. A multi-zone kinetic model can be useful to simulate the reactors where the reactions occur with multiple interfaces with transient rate parameters. In the BOF process, it is evident that the overall kinetics can be successfully simulated by a multiple zone reaction approach by use of time variant rate parameters as a function of process dynamics.
2. The model predicts that the significant share of refining in a BOF process is caused by the recirculation of metal fragments through the emulsion zone. The number of metal droplets ejected, size and time of residence of droplets in the emulsion and the equilibrium concentration at the interface of the droplet are the primary factors that

decide the refining kinetics in the emulsion phase. The large thermodynamic driving force of droplets during the initial stage of blowing is responsible for high refining rate of Si, Mn and P.

3. It is predicted that the reaction rates of Si, Mn and P refining in the droplet are fast and approaches equilibrium within a few seconds inside the emulsion. The oxidation rate of C is influenced by the initial droplet size.
4. The metal drops in the lower region of size spectrum make a significant contribution to the conversion process in the emulsion zone.
5. The formation of Fe_tO in the slag is highly interlinked with the post combustion ratio. A dynamic post-combustion model, particularly during the early and end blow period is useful for accurate prediction of Fe_tO evolution in slag.

We recommend that experimental work on studying the detailed kinetics of the reactions of Fe-C-Si-Mn-P in an oxidising slag will provide greater knowledge of kinetics of steelmaking process. Future work on developing a heat balance model, focusing on evaluating the macroscopic heat transfer of recirculating metal drops and coupling with the present kinetic model can provide a detailed insight of the BOF reactions.

Acknowledgements

The authors wish to acknowledge the financial support provided by Tata Steel to carry out this research work. BKR would like to thank Mariana Adderley for the constructive and helpful discussion regarding this work.

List of symbols and abbreviations

A-Interfacial area (m^2)
C_{jm} – Concentration of j^{th} component in metal, j = Si, C, Mn and P (wt %)
C_{ji} – Concentration of j^{th} component on the reaction interface (wt %)

816 C_{jd}^{return} – Concentration of jth component of refining droplets (wt %)
817 $C_{p,m}$ – Heat capacity of bulk metal (J/kg)
818 $C_{p,s}$ – Heat capacity of slag (J/kg)
819 d_p – Diameter of the droplet (m)
820 D– Diffusion coefficient of slag (m^2/s)
821 $F_{G,T}$- Temperature corrected oxygen flow rate (Nm^3/min)
822 h- Height of the cavity (m)
823 k_a- Apparent rate constant (mole/m^2.s.atm)
824 k_g- Gas phase mass transfer coefficient (mole/m^2.s.atm)
825 k_d^{em}- Overall mass transfer coefficient of droplet (m/s)
826 k_{jm}^{d}- Mass transfer coefficient in metal side of droplet (m/s)
827 k_s^{d}- Mass transfer coefficient in slag side of droplet (m/s)
828 k_m^{sm}- Overall mass transfer coefficient at slag-bulk metal interface (m/s)
829 k_m^{gm}- Mass transfer coefficient in the melt in jet impact area (m/s)
830 L_h – Lance height (between lance tip and bath surface (m)
831 m_d- Mass of a single droplet (kg)
832 $m_{d,p}$- Average mass of droplets belongs to pth size class (kg)
833 m_d^{return}- Weight of a single droplet returns to the bath (kg)
834 M – Molecular weight (g/mole)
835 $N_p^{eject,t}$ – Number of droplets of pth class size ejects to the bath at blowing time t (-)
836 $N_p^{return,t}$ – Number of droplets of pth class size returns to the bath at blowing time t (-)
837 $N_{B,T}$- Modified blowing number (-)
838 P^b_{CO2} –Partial pressure of CO_2 (atm)
839 P^b_{O2} –Partial pressure of O_2 (atm)
840 PCR- Post combustion ratio (-)
841 Re- Reynolds number (-)
842 $R_{B,T}$- Droplet generation rate (kg/min)
843 Sh - Sherwood number (-)
844 Sc- Schmidt number (-)
845 r_c – Decarburization rate of the droplet (wt pct/s)
846 r_c^* – Critical decarburization for bloating (wt pct/s)
847 r_{cav} – Cavity radius (m)
848 t_c – Contact time between the metal droplet and slag (s)
849 t_{res} – Residence time of droplet in emulsion (s)
850 T_s- Interface temperature at slag-metal (K)
851 T_∞- Temperature in the emulsion medium (K)
852 T_0- Initial temperature of the metal drop at the time of ejection (K)
853 u – Velocity of the droplet (m/s)
854 V_d- Volume of droplet (m^3)
855 W_c- Weight of carbon (kg)
856 WC_j- Weight of impurity (kg)]
857 W_D- Weight of dolomite (kg)
858 $W_{d,p}$- Weight proportion of droplet belongs to pth size class (kg)
859 W_L- Weight of lime (kg)
860 W_m- Weight of hot metal, (kg)
861 $\Delta W_{m,ref}^t$- Weight of refining hot metal in a numerical time step (kg)
862 ΔW_{MOx} – Sum of oxide mass in a numerical time step (kg)
863 W_s- Weight of slag, (kg)

W_{jm}^{eject}- Weight of jth element in the hot metal ejected to the emulsion (kg)
W_{jm}^{return}- Weight of jth element in the hot metal return to the bath (kg)
W_{sc}^{m} - Weight of the melted scrap (kg)

Greek symbols

ρ_d – Density of droplet (kg/m^3)
$\rho_{d,0}$ – Initial density of droplet (kg/m^3)
ρ_m – Density of the bulk metal (kg/m^3)
ρ_s – Density of slag (kg/m^3)
λ_m- Thermal conductivity of liquid metal (W/mK)
λ_s- Thermal conductivity of slag (W/mK)

Subscripts and Superscripts

cav- Cavity
d- droplet
m- Hot metal
P- Number of classes in the droplet size spectrum
eq- Equilibrium
hs- Hot spot
iz- Impact zone
em- Emulsion
sm- Slag/metal
gm- Gas/metal

References

1. W. Knoop, B. Deo, A. Snoeijer, G. Unen and R. Boom: *InProceedings of the 4th International Conference on Molten Slags and Fluxes, ISIJ*, Tokyo 1992, pp. 302-307.

2. H. Jalkanen and L. Holappa: *VII International Conference on Molten Slags Fluxes and Salts, The South African Institute of Mining and Metallurgy*, 2004, pp. 71-76.

3. A. K. Shukla, B. Deo, S. Millman, B. Snoeijer, A. Overbosch and A. Kapilashrami: *Steel Research International*, 2010, vol. 81, pp. 940-48.

4. I. H. Jung, P. Hudon, M. A. Van Ende and W.Y. Kim: *AISTech-Iron and Steel Technology Conference Proceedings*, 2014, vol 1, pp. 1257-68.

5. N. Dogan, G. A. Brooks and M. A. Rhamdhani: *ISIJ Int.*, 2011, vol. 51(7), pp. 1086-92.

6. F. Pahlevani, S. Kitamura, H. Shibata and N. Maruoka: *Steel Res. Int.*, 2010, vol. 81, pp. 617-22.

7. Y. Ogasawara, Y. Miki, Y. Uchida and N. Kikuchi, *ISIJ Int.*, 2013, vol. 53, pp. 1786-93.

8. R. Sarkar, P. Gupta, S. Basu and N. B. Ballal: *Metall. Mater. Trans. B*, 2015, vol. 46, pp. 961-76.

9. C. Kattenbelt and B. Roffel: *Metall.Mater. Trans. B*, 2008, vol. 39, pp. 764-69.

10. Y. Lytvynyuk, J. Schenk, M. Hiebler and A. Sormann: *Steel Research International* 2014, vol. 85, pp. 537-43.

11. D. Guo, D. Swickard and J. Bradley: *Iron Steel Technol., Apr* 2014, pp. 131-40.

12. G. Li, B. Wang, Q. Liu, X. Tian, R. Zhu, L. Hu and G. Cheng: *International Journal of Minerals, Metallurgy, and Materials* 2010, vol. 17, pp. 715-22.

13. G. Brooks N. Sasaki, M. A. Rhamdhani: *Asia Steel*, Yokihama, Japan, 2015.

14. S. Kitamura: *Steel Research International* 2010, vol. 81, pp. 766-71.

15. S. Ohguchi, D. G. C. Robertson, B. Deo, P. Grieveson and J. H. E. Jeffes: *Ironmak Steelmak.*, 1984, vol. 11, pp. 202-13.

16. G. A. Brooks, M. A. Rhamdhani, K. S. Coley, Subagyo and Y. Pan: *Metall. Mater. Trans. B*, 2009, vol. 40B, pp. 353-62.

17. A. Kirindigoda Hewage, B. K. Rout, G. Brooks and J. Naser: *Ironmak. Steelmak.* 2016, vol. 43, pp. 358-70.

18. M. S. Millman, A. Kapilashrami, M. Bramming and D. Malmberg: *Imphos: Improving Phosphorus Refining*, European Union, Luxembourg, 2011.

19. B. K. Rout, G. A. Brooks, Z. Li and M. A. Rhamdhani: *AISTech - Iron and Steel Technology Conference Proceedings*, 2015, vol. 3, pp. 3225-37.

20. B. K. Rout, G. Brooks, M. A. Rhamdhani, Z. Li, F. N. H. Schrama and A. Overbosch: *Metall. Mater. Trans. B* (submitted, E-TP-17-603-B), 2017.

21. B. K. Rout, G. Brooks, M. A. Rhamdhani, Z. Li, F.Schrama and W.van der Knoop: *Metall. Mater. Trans. B* (submitted, E-TP-17-604-B), 2017

22. Q. Li, M. Li, S. Kuang, & Z. Zou : *Metall. Mater. Trans. B.* , 2015, vol. 46, pp.1494-1509.

23. S. Kitamura, T. Kitamura, K. Shibata, Y. Mizukami, S. Mukawa, and J. Nakagawa: *ISIJ Int.,1991,* vol 31, no. 11, pp. 1322-1328.

24. N. Dogan, G. A. Brooks and M. A. Rhamdhani: *ISIJ Int.* 2011, vol. 51(7), pp. 1102-09.

25. K. Chou, U. B. Pal and R. G. Reddy: *ISIJ Int.*, 1993, vol. 33, pp. 862-68.

26. B. Deo and R. Boom: *Fundamentals of Steelmaking Metallurgy*, Prentice Hall, Hertfordshire,1993, pp. 194.

27. B. K. Rout, G. A. Brooks, Z. Li and M. A. Rhamdhani: *AISTech - Iron and Steel Technology Conference Proceedings*, 2016, vol. 1, pp 1019-26.

28. F. R Cheslak, J. A. Nicholls and M. Sichel: *Journal of Fluid Mechanics* 1969, vol. 36, pp. 55-63.

29. S. C. Koria and K. W. Lange: *Steel Res.* 1987, vol. 58, pp. 421-26.

30. P. Kozakevitch: *J Metals*, 1968, vol. 22, pp. 57-67.

31. H. W. Meyer, W. F. Porter, G. C. Smith and J. Szekely: *J Metals*, 1968, vol. 20, pp. 35-42.

32. G. Brooks, Y. H. Pan, Subagyo and K. Coley: *Metall. Mater. Trans. B*, 2005, vol. 36, pp. 525-35.

946 33. C. L. Molloseau and R. J. Fruehan: *Metall. Mater. Trans. B,* 2002, vol. 33, pp. 335-
947 44.

948 34. H. Gaye and P. V. Riboud: *Metallurgical Transactions B,* 1977, vol. 8, pp. 409-15.

949 35. P. Kozakevitch, G. H. Geiger, M. Olette and P. V. Riboud: *BOF Steelmaking,* Iron
950 and Steel Society, 1975, vol 2, chapt. V, pp. 287-88.

951 36. K. Gu, N. Dogan and K. S. Coley, *Metall. Mater. Trans. B, 2017*, pp. 1-18.

952 37. H. Sun, and G. Zhang, *AISTech - Iron and Steel Technology Conference Proceedings*,
953 2005, pp 257–268.

954 38. K. Gu, N. Dogan and K. S. Coley: *Metall. Mater. Trans. B,* 2017, vol. 48, pp. 2343-
955 2353.

956 39. F. D. Richardson: *Physical chemistry of melts in metallurgy*. Academic Press
957 (Elsevier), 1974, vol. 2, pp. 412-416.

958 40. F. Oeters : *Metallurgy of steelmaking*. Verlag Stahleisen, 1994, pp. 369.

959 41. C. P. Manning and R. J. Fruehan: *Metall. Trans. B,* 2013, vol. 44B, pp. 37-44

960 42. S. Ban-Ya: *ISIJ Int.* 1993, vol. 33, pp. 2-11.

961 43. K. Narita, T. Makino, H. Matsumoto, A. Hikosaka and J. Katsuda: *Tetsu-to-Hagané*
962 1983, vol. 69, pp. 1722-29.

963 44. H. Suito and R. Inoue: *ISIJ Int.,* 1995, vol. 35, pp. 266-71.

964 45. C. Cicutti, M. Valdez, T. Pérez, J. Petroni, A. Gómez, R. Donayo and L. Ferro: *Sixth*
965 *International Conference on Molten Slags, Fluxes and Salts*, ed. ISS (Stockholm-Helsinki:
966 Warrandale, PA, 2000).

967 46. S. C. Koria and K. W. Lange: *Metall. Trans. B,* 1984, vol. 15, pp. 109-16.

968 47. B. K. Rout, G. A. Brooks, M. A. Rhamdhani and Z. Li: *Metall.Mater. Trans. B*, 2016,
969 vol 47 (6), pp. 3350-61.

970 48. Subagyo, G. Brooks, K. S. Coley and G. A. Irons: *ISIJ Int.,* 2003, vol. 43 (7), pp. 983-
971 89.

972 49. Subagyo, G. Brooks, and K. Coley: *Canadian Metallurgical Quarterly*, 2005, vol. *44*(1),
973 pp. 119–129.

974 50. Y. Doh, P. Chapelle, A. Jardy, G. Djambazov, K Pericleous, G Ghazal and P Gardin:
975 *Metall. Mater. Trans. B* 2013, vol. 44, pp. 653-70.

976 51. B. T. Chao, *Journal of Heat Transfer* 1969, vol. 91, pp. 273-80.

977 52. P. Sulasalmi, V. Ville-Valtteri, A. Kärnä, M. Järvinen, S. Ollila, and T.
978 Fabritius: *Metall.Mater. Trans. B,* 2016, vol. 47(6), pp: 3544-3556.

979 53. T. Nishi, H. Shibata, Y. Wasedaand H. Ohta: *Metall.Mater. Trans. A*, 2003, vol.
980 34(12), pp.2801-2807.

981 54. K. Nishioka, T. Maeda, M. Shimizu: *ISIJ Int.*, 2006, vol. 46(3), pp.427-33.

982 55. N. Dogan, G. A. Brooks, and M. A. Rhamdhani: *ISIJ Int.*, 2009, vol. *49*(10), 1474–1482.

983 56. http://www.factsage.com/

984 57. E. Schürmann, K. Obst, L. Fiege and H. Kaiser: *Steel Res. Int.*, 1985, vol. 56, pp. 425-
985 31.
986 58. M. Hirai, R. Tsujino, T. Mukai, T. Harada and M. Omori: *Trans.ISIJ,* 1987, vol.
987 27(10), pp. 805-813.

988 59. S. Li, X. Wei and L. Yu: *Fuel*, 2011, vol. 90, pp. 1350-60.

989 60. K. Ito and R. J. Fruehan: *Metall. Tans. B*, 1989, vol. 20, pp. 509-14.

990 61. Slag Atlas, *Verlag Stahleisen GmbH, Düsseldorf* 1995, pp. 345-346.

991 62. A. Kondratiev and E. Jak: *Metall. Mater. Trans. B*, 2001, vol. 32, pp. 1015-25.

992 63. K Chiba, A Ono, M Saeki, M Yamauchi, M Kanamoto and T Ohno: *Ironmak.*
993 *Steelmak.*, 1993, vol. 20, pp. 215-20.

994 64. F. E. Rote and R. A. Flinn: *Metall. Trans.*, 1972, vol. 3, pp. 1373-84.

995 65. Y. E. Lee and L. Kolbeinsen: *ISIJ Int.* 2007, vol. 47, pp. 764-65.

996 66. M. Ishiguro: *Tetsu-to-Hagane*, 1971, vol. 57, pp. 267-70.

997 67. S. C. Koria and K. W. Lange: *Steel Res.* 1987, vol. 58, pp. 421-26

998 68. S. Ban-Ya: *ISIJ Int.*, 1993, vol. 33, pp. 2-11.

999 **Appendix:**

1000

A.1. Mass transfer coefficient in hot metal and slag

1001 The mass transfer coefficient in the hot metal has been calculated by the following
1002 relationship [23],

$$\log k_m = 1.98 + 0.5 \log\left(\frac{\varepsilon H^2}{100L}\right) - \frac{125000}{2.3RT} \quad \text{(A1)}$$

1003 where k_m is the mass transfer coefficient in metal phase (cm/s), ε is the stirring energy (W/t),
1004 H and L are the bath depth (cm) and diameter of the furnace respectively and T is the
1005 temperature in the impact zone (K). The total stirring energy was calculated by using the
1006 combined effect of the top and bottom gas injection in the BOF. [67]

1007 The slag phase mass transfer coefficient was given by: [7]

$$k_s = a \exp\left(-\frac{37000}{RT}\right).\varepsilon^b \quad \text{(A2)}$$

Where k_s is the mass transfer coefficient in slag phase (cm/s), R: gas constant ($J.mol^{-1}K^{-1}$), a and b are the empirical parameters, assumed to be 1.7 and 0.25 respectively.[7]

A.2. Calculation of cavity height and radius:

The height and radius of the individual cavity formed by the top jet can be expressed as:

$$h = 4.469\, \dot{M}_h^{0.66} L_h \#(A3)$$

$$r_{cav} = 0.5 \times 2.813 L_h \dot{M}_d^{0.282} \#(A4)$$

Where L_h is the lance height (m) and the dimensionless momentum flow rate $\dot{M}_h$ and $\dot{M}_d$is defined as:

$$\dot{M}_h = \frac{\dot{m}_n \cos(nangle)}{\rho_m g L_h^3} \#(A5)$$

$$\dot{M}_d = \frac{\dot{m}_t(1+\sin(nangle))}{g\rho_m L_h^3} \#(A6)$$

Where $\dot{m}_n$ is the momentum flow rate of the each nozzle, which is related to the total meomentum flow rate, $\dot{m}_t$ by the following equations:

$$\dot{m}_n = \frac{\dot{m}_t}{n_n} \#(A7)$$

Total momentum flow rate:

$$\dot{m}_t = 0.7854 \times 10^5 \times n_n \times d_{th}^2 \times P_a \left(\frac{1.27 P_0}{P_a} - 1\right) \#(A8)$$

Where, n_n is the number of nozzles in the lance tip, nangle is the nozzle angle (rad), d_{th} is the throat diameter of the lance (m), P_0 is the top supply pressure (Pa) and P_a is the ambient pressure (Pa).

A.3. Calculation of equilibrium distribution ratios

1025

Silicon distribution ratio[42]:

$$L_{Si} = \begin{cases} 1 - \dfrac{(\%FeO)}{40}, & (\%FeO) \leq 40 \\ 0, & \%FeO) > 40 \end{cases} \quad \text{(A9)}$$

1026

Manganese distribution ratio: [43]

$$\begin{aligned} \log k'_{Mn} = -0.0180[&(wt\ pct\ CaO) + 0.23(wt\ pct\ MgO) \\ &+ 0.28(wt\ pct\ Fe_tO) - 0.98(wt\ pct\ SiO_2) \\ &- 0.08(wt\ pct\ P_2O_5)] + \frac{7300}{T} - 2.697 \end{aligned} \quad \text{(A10)}$$

1027 Where the apparent equilibrium constant k'_{Mn} is defined as:

$$k'_{Mn} = \frac{(wt\ pct\ MnO)}{(wt\ pct\ T.Fe)\times[wt\ pct\ Mn]} = \frac{L_{Mn}\times\frac{M_{Mn}}{M_{MnO}}}{(wt\ pct\ T.Fe)} \quad \text{(A11)}$$

1028 T.Fe- total Fe and M_{Mn} and M_{MnO} are the molar mass (g/mol) of Mn and MnO respectively.
1029

Phosphorus distribution ratio:

1030 The phosphorus equilibrium distriburtion ratio at the slag-metal interface can be written as[68]:

$$L_p = \frac{K_p f_p h_o^{2.5}}{C\gamma_{PO_{2.5}}} \quad \text{(A12)}$$

1031 Where, K_p is the equilibrium constant, f_p is the activity coefficient of P, h_o is the heneraian
1032 activity of oxygen, C is the conversion factor which related (%P) with the mole fraction of
1033 $PO_{2.5}$ and γ_{p2o5} is the activity coefficient of $PO_{2.5}$

1034 The equilibrium constant for the phosphorus oxidation reaction can be expressed as[63]:

$$\log(K_p) = \frac{17060}{T} - 8.51 \quad \text{(A13)}$$

1035 Here, ho is the henerian activity of oxygen, determined by assuming FeO-O equilibrium.

$$h_o = \frac{\gamma_{FeO}}{X_{FeO} K_F} \quad \text{(A14)}$$

K_F is the equilibrium constant for reaction [Fe] +[O] = (FeO), ΔG^o = -128090+57.99 T.[63] γ_{Feo} and γ_{p2o5} are the activity coefficient of FeO and $PO_{2.5}$, determined by Regular solution model proposed by Ban-Ya.[40] Henerian activity coefficient f_p was determined by employing the first order interaction parameter.$\log(f_p) = e_p^p[\%P] + e_p^c[\%C]$

Where e_p^p = 0.063 and e_p^c =0.19.[7]

Caption List

Figure Captions

Figure 1: Schematic representation of reactions in BOF converter

Figure 2: Schematic representation of the refining mechanism in the emulsion zone

Figure 3: Proposed refining mechanism of metal droplets in the slag-metal emulsion

Figure 4: Model for Fe_tO evolution during blowing period

Figure 5: Post-combustion profile used for Fe_tO generation model. PCR- (post-combustion ratio)

Figure 6: A three zone kinetic model for prediction of metal and slag composition during blowing period of a top/combined blowing steelmaking converter process

Figure 7: Algorithm for BOF dynamic model

Figure 8: Model prediction of carbon concentration variation as a function of blowing time with different computational time steps

Figure 9: Temperature change across various reaction interfaces inside the furnace during the blowing time

Figure 10: Removal kinetics of C, Si, Mn and P of a single metal drop in emulsion (a) Initial droplet diameter = 6×10^{-4} m (b) Initial droplet diameter = 9×10^{-4} m

Figure 11: Model prediction of hot metal composition (wt pct) during the blowing period. (a) Carbon, (b) Silicon, (c) Manganese, (d) Phosphorus

Figure 12: Evolution of slag composition (wt pct) during blowing period. (a) SiO_2, (b) Fe_tO, (c) MnO, (d) P_2O_5, (e) CaO, (f) MgO.

Figure 13: Variation of hot metal and slag weight during the blowing period as predicted by the model for PCR profile 1

List of Tables:

Table 1: Impurities removed in different zones of a BOF converter

Reaction zone	**Impurities removed**
Jet impact (hot spot)	C, Si, Mn
Slag-bulk metal	C, Si, Mn, and P
Slag-metal emulsion	C, Si, Mn and P

Table 2: Rate equations in three different zones of the converter

Reaction zone	**Rate equations**	**Model parameters**
Jet impact zone (gas-metal)	$\left.\frac{d(W_m C_{jm})}{dt}\right\|_{iz} = -A_{iz} k_m^{gm} \rho_m \left(C_{jm} - C_{ji}^{gm} \right)$ (1) j = Si, Mn, P and C ≤ 0.3 wt pct. For C oxidation, C > 0.3 wt pct: $\left(\frac{dW_c}{dt}\right)_{iz} = \left(\frac{dW_c}{dt}\right)^{CO_2}{}_{iz} + \left(\frac{dW_c}{dt}\right)^{O_2}{}_{iz}$ (2) $\left(\frac{dW_c}{dt}\right)^{CO_2}{}_{iz} = -100 \times M_C A_{iz} k_a P_{CO_2}^b$ (3)	Jet impact area – A_{iz}, gas/metal interface concentration- C_{ji}^{gm}, mass transfer coefficients - k_m^{gm}, k_g, k_a

	$\left(\frac{dW_c}{dt}\right)^{O_2}{}_{iz} = -200 \times M_C A_{iz} k_g (1 + P_{O_2}^b)$ (4)	
Slag-bulk metal (slag-metal)	$\left.\frac{d(W_m C_{jm})}{dt}\right\|_{sm} = -A_{sm} k_m^{sm} \rho_m \left(C_{jm} - C_{ji}^{sm} \right)$ (5)	Slag-bulk metal area – A_{sm}, slag/metal interfacial concentration- C_{ji}^{sm}, mass transfer coefficient -k_m^{sm}
Slag-metal emulsion (slag-metal drops)	Rate of mass transfer between metal drops and slag: $\left.\frac{d(m_d C_{jd})}{dt}\right\|_{em} = -A_d k_d^{em} \rho_m \left(C_{jd} - C_{ji}^{em} \right)$ (6) Rate of refining of bulk metal by emulsion: $\left.\frac{d(W_m C_{jm})}{dt}\right\|_{em} = -\frac{W_{jm}^{eject,t} - W_{jm}^{return,t}}{\Delta t}$ (7) $W_{jm}^{eject,t} = \left(\sum_{p=1}^{P} \left(R_{B,T}\right)_p \times \Delta t \right) \times \frac{C_{jm}^t}{100}$ (8) $W_{jm}^{return,t} = \sum_{p=1}^{P} N^{return,t}{}_p \times \frac{\left(C_{jd}^{return,t} m_d^{return,t}\right)_p}{100}$ (9) $N_p^{return,t} = N_p^{eject,t-t_{res}} = \frac{W_{d,p}^{t-t_{res}}}{\bar{m}_{d,p}}$ (10)	Interfacial area of droplet– A_d, residence time of drops in emulsion- t_{res}, mass transfer coefficient– k_d^{em}, droplet generation rate- $R_{B,T}$,metal droplet concentration- C_{jd} interfacial concentration at metal drop/slag interface-C_{ji}^{em}, $\bar{m}_{d,p}$- average droplet mass of size class p (p – droplet size class, P -total number of classes in the droplet size spectrum; Please refer section 1.2.1.5)

1077 Table 3: Estimation of interfacial concentration at slag-metal interface

Reactions	**Interface concentration at slag/metal phase boundary**	**Method**
Carbon $[C] + (FeO) = \{CO\} + [Fe]$	$[\%C]_{eq} = \frac{P_{CO} \times a_{Fe}}{f_c \times a_{FeO} \times K_c}$	P_{CO}- 1.5×10^5 Pa, a_{Fe} = 1, f_c- empirical correlation[25], a_{FeO}- Regular solution model[39], Equilibrium constant: $\log(K_c) = 5.096 - \frac{5730}{T_m}$
Silicon $[Si] + (FeO) = (SiO_2) + [Fe]$	$[\%Si]_i = L_{Si}^* \times [\%Si]$	L_{Si}^* – Narita *et al.*[41]

Manganese $[Mn] + (FeO) = (MnO) + [Fe]$	$[\%Mn]_i = \frac{(\%Mn)}{L_{Mn}}$	L_{Mn}- Suito *et al.*[42]
Phosphorus $2[P] + 5(FeO) = (P_2O_5) + 5[Fe]$	$[\%P]_i = \frac{(\%P)}{L_p}$	L_p-Regular solution model[39]

1078

1079 Table 4: Thermal properties of steel and slag used in the model for the calculation of surface
1080 temperature of metal droplet

	Steel	**Slag**			
		FeO	**SiO_2**	**CaO**	**MnO**
Heat capacity (J/kg K)[52]	821	947	1429.5	928	854.5
Thermal conductivity (W/mK)	40[53]	1.7[54]			

1081

1082 Table 5: Model input parameters

Input parameters	**Value**
Initial hot metal composition (Blowing time = 2.2 min)	170000 kg, wt pct C= 3.86, wt pct Si = 0.19, wt pct Mn = 0.29, wt pct P = 0.065
Scrap composition	30000 kg, wt pct C = 0.08, wt pct Si = 0.001, wt pct Mn = 0.52
Hot metal temperature	1623- 1923 K (1350- 1650 °C)
Initial slag composition and weight	Initial slag weight at 2.2 min = 5200 kg, total lime added = 7600 kg, Iron ore = 1900 kg, Quartzite = 800 kg Slag composition : wt pct CaO = 27, wt pct FeO = 33, wt pct SiO_2 = 17, wt pct MnO = 13.5, wt pct MgO = 5, wt pct P_2O_5= 3.5
Oxygen blow	620 Nm^3/min, six hole lance
Bottom blow (Ar/N_2)	2.5 – 8.33 m^3/min
Lance height	2.5, 2.2, 1.8 m

Steel density	7000 kg/m^3
Slag density	Partial molar volume method [61]
Surface tension of steel	1.7 N/m
Viscosity of slag	Modified Urbain model [62]
Diffusion coefficient in metal phase at 1873K (1600 °C)	C- 2.0 × 10^{-9} m^2/s , Si – 3.8× 10^{-9} m^2/s, Mn – 3.7× 10^{-9} m^2/s, P-4.7× 10^{-9} m^2/s
Gas fraction in emulsion	0.8
Diameter of initial droplets	0.00023 - 0.00335 m, 10 classes
Angle of droplet ejection	60 degree

1083